Markowski, P., M. Majcen, Y. Richardson, J. Marquis, and J. Wurman, 2011: Characteristics of the wind field in a trio of nontornadic low-level mesocyclones observed by the Doppler on Wheels radars. *Electronic J. Severe Storms Meteor.*, **6** (3), 1–48.

Electronic Journal of
SEVERE STORMS METEOROLOGY

Characteristics of the Wind Field in Three Nontornadic Low-Level Mesocyclones Observed by the Doppler on Wheels Radars

PAUL MARKOWSKI, MARIO MAJCEN, YVETTE RICHARDSON, AND JIM MARQUIS
Department of Meteorology, The Pennsylvania State University, University Park, Pennsylvania

JOSHUA WURMAN
Center for Severe Weather Research, Boulder, Colorado

(Submitted 27 August 2010; in final form 09 April 2011)

ABSTRACT

The three-dimensional wind fields within three nontornadic supercell thunderstorms are retrieved from dual-Doppler radar observations obtained by a pair of Doppler on Wheels (DOW) radars. The observations focus on the low-level mesocyclone regions of the storms near the time of strongest low-level rotation. All three storms display strong low-level rotation (e.g., the vertical vorticity maxima exceed 0.05 s^{-1} in the lowest 1000 m AGL in each storm). A principal finding is that the nontornadic mesocyclones possess many of the same signatures found in tornadic supercells, even those viewed in similarly fine resolution; e.g., rear-flank gust fronts wrapping around the circulation centers, multiple cyclonic vertical vorticity maxima along the gust front that spiral inward toward the circulation center, and arching vortex lines joining the cyclonic vorticity maxima to regions of anticyclonic vertical vorticity on the opposite side of the hook echo. The nontornadic mesocyclones possess less circulation than most of the tornadic mesocyclones that have been observed by the DOW radars, particularly within 1 km of the axis of rotation. Another finding is that the trajectories of air parcels passing through the near-surface vertical vorticity maxima have relatively shallow upward vertical excursions, suggesting that these parcels do not enter the overlying midlevel updraft and mesocyclone.

1. Introduction

The challenge of discriminating between tornadic and nontornadic mesocyclones probably has been the biggest motivation for studying supercell storms. In the United States, tornado-warning decisions rely heavily on single-Doppler radar observations, such as those provided by the WSR-88D. Recent estimates are that only about 25% of mesocyclones detected by WSR-88D are associated with tornadoes (Trapp et al. 2005).[1] Not only is mesocyclone detection of limited value in alerting forecasters to the possibility of a tornado, but even mesocyclone strength (quantified in single-Doppler data in terms of azimuthal shear or differences between maximum inbound and outbound radial velocities) is only a mediocre predictor of the possibility of a tornado (Wakimoto et al. 2004a; Trapp et al. 2005), which develops on a smaller scale than the parent mesocyclone.

Corresponding author address:
Paul Markowski, Department of Meteorology,
The Pennsylvania State University,
520 Walker Building,
University Park, PA 16802
E-mail: pmarkowski@psu.edu

[1]Trapp et al. (2005) used relatively strict criteria to identify circulations as mesocyclones. If less stringent strength thresholds are used, then the percentage of mesocyclones that are tornadic decreases accordingly.

Table 1: Prior studies documenting dual-Doppler observations of nontornadic low-level mesocyclones.

Date	Location	References
6 Jun 1974	central Oklahoma	Brandes (1977)
20 May 1977	central Oklahoma (the "Hailstorm" north of Del City)	Ray et al. (1981)
19 Jun 1980	central Oklahoma	Vasiloff et al. (1986)
2 Aug 1981	southeastern Montana	Miller et al. (1988)
26 Apr 1984	central Oklahoma	Bluestein and Woodall (1990)
12 May 1985	central Oklahoma	Marwitz and Burgess (1994)
29 May 1994	near Graham, TX	Ziegler et al. (2001)
29 Apr 1995	near Sherman, TX	Trapp (1999); Markowski et al. (2008)
12 May 1995	near Hays, KS	Trapp (1999); Wakimoto and Cai (2000); Markowski et al. (2008)
22 May 1995	near Shamrock, TX	Trapp (1999); Bluestein and Gaddy (2001); Markowski et al. (2008)
24 May 2000	Kanto Plain, Japan	Shimizu et al. (2008)
29 May 2001	near Kress, TX	Beck et al. (2006)
23 May 2002	Lipscomb County, TX	Frame et al. (2009)
23 Jun 2003	near Superior, NE	Wakimoto et al. (2004)

Although supercells often are idealized as being quasi-steady, actual supercells can be very unsteady, especially at low levels. For example, a long-lived supercell can develop multiple low-level mesocyclones cyclically (Burgess et al. 1982; Adlerman et al. 1999; Dowell and Bluestein 2002a,b). Thus, it is possible for a supercell, and perhaps even a midlevel mesocyclone, to be associated with both tornadic and nontornadic low-level mesocyclones over the storm's lifetime, which makes the terms *tornadic supercell* and *nontornadic supercell* somewhat ambiguous. For this reason, we will refer to *low-level mesocyclones* as being tornadic or nontornadic whenever possible. The terms *tornadic supercell* and *nontornadic supercell* will be used sparingly; a supercell that produces at least one tornado will qualify for the former label, and the latter label will be reserved for a supercell that produces no known tornadoes throughout its lifetime.

In contrast to the typical operational setting, in field experiments it is often possible to retrieve the three-dimensional wind field by scanning regions nearly simultaneously from different angles, using multiple radars. This knowledge of the three-dimensional wind field obviously offers many advantages over observations of only radial winds. Unfortunately, dual-Doppler observations of supercells are relatively rare, especially observations affording a relatively high-resolution (e.g., coarsest data spacing <250 m and volumes every 1-2 min in the region of interest) examination of storm characteristics at low levels, especially the lowest 500 m AGL. Although nontornadic mesocyclones are much more common than tornadic mesocyclones, analyses of the latter are more prolific in the peer-reviewed literature.

Table 1 lists 14 peer-reviewed cases of dual-Doppler wind syntheses in nontornadic low-level mesocyclones, without regard for data quality or the investigators' objectives. Though we have made every attempt to identify past nontornadic cases, Table 1 almost certainly is incomplete. Nonetheless, we see a shortage of nontornadic low-level mesocyclone analyses, particularly those that can resolve motions having scales smaller than the mesocyclone or confined to within the lowest few hundred meters above the ground.

The near-surface, *submesocyclone* scale has not been observed well in prior studies, which usually have analyzed either pseudo-dual-Doppler airborne radar observations [most during the first Verification of the Origins of Rotation in Tornadoes Experiment (hereafter VORTEX1; Rasmussen et al. 1994), in 1994–1995; e.g., Wakimoto and Atkins 1996; Wakimoto and Liu 1998; Wakimoto et al. 1998; Trapp 1999; Wakimoto and Cai 2000; Bluestein and Gaddy 2001; Ziegler et al. 2001; Dowell and Bluestein 2002a,b; Wakimoto et al. 2004b; Markowski 2008; Markowski et al. 2008] or data from fixed radar networks (mostly in the 1970s

and 1980s; e.g., Ray et al. 1975, 1981; Ray 1976; Brandes 1977, 1978, 1981, 1984; Heymsfield 1978). A steady state must be assumed for relatively long time periods (typically 5–7 min) when analyzing dual-Doppler observations from airborne radars, Additionally their resolution is coarser than that of ground-based mobile radars because 1) aircraft must maintain larger distances from the mesocyclone in the interest of safety, and 2) ground clutter contaminates observations within a few hundred meters of the ground. The baselines of fixed, ground-based dual-Doppler networks are usually long (commonly 40–60 km); thus, the centers of the dual-Doppler lobes, where the geometry is most favorable for accurate wind retrievals, are at a large range from the radars. This results in relatively coarse resolution and an inability to observe the lowest few hundred meters, owing to radar-horizon limitations.

One of the principal findings of VORTEX1 was the striking similarity of the kinematic structure of tornadic and nontornadic mesocyclones on the mesocyclone scale (e.g., Trapp 1999; Wakimoto and Cai 2000; Markowski et al. 2008). Trapp (1999) compared pseudo-dual-Doppler analyses of three tornadic and three nontornadic supercells observed by X-band airborne Doppler radar mounted on the NOAA P-3 aircraft (the only dual-Doppler observations of supercells in VORTEX1 being airborne). Trapp found that both tornadic and nontornadic supercells had mesocyclones in the lowest several hundred meters AGL; thus, the existence of a low-level mesocyclone was insufficient for tornadogenesis. The nontornadic mesocyclones had a larger radius of maximum tangential wind than the tornadic mesocyclones as a result of less horizontal convergence and vorticity stretching.

Wakimoto and Cai (2000) analyzed a nontornadic supercell that was observed by the (airborne, X-band) Electra Doppler radar (ELDORA; Hildebrand et al. 1994, 1996; Wakimoto et al. 1996) on 12 May 1995 near Hays, KS. The low-level mesocyclone was compared to a tornadic low-level mesocyclone observed by the ELDORA on 16 May 1995 near Garden City, KS (Wakimoto et al. 1998; Wakimoto and Liu 1998). Wakimoto and Cai (2000) concluded that the two supercells had remarkably similar kinematic structure (e.g., see their Fig. 15). Based on the features that could be resolved, the updraft and the downdraft structures were very similar, and the vertical vorticity associated with low-level mesocyclones was approximately equal in strength and found in similar location relative to the respective updrafts. The only differences, they noted, were greater intensity of: 1) precipitation echoes behind the rear-flank gust front, 2) storm-relative inflow, and 3) updrafts and vertical vorticity along the rear-flank gust front in the nontornadic (Hays) case.

Markowski et al. (2008) investigated the configurations of vortex lines in tornadic and nontornadic low-level mesocyclones, also using airborne pseudo-dual-Doppler radar data from VORTEX1 (from the NOAA P-3 and ELDORA). They found that the vertical vorticity dipoles commonly observed straddling the hook echo and rear-flank downdraft (RFD) of supercells were joined by vortex line "arches" in every case, both tornadic and nontornadic. They argued that the vortex line configurations—not only the arching structures, but also the fact that the horizontal projections of the vortex lines implied horizontal vorticity of a 90–180° different orientation than that associated with the environmental wind shear—strongly implied that baroclinic vorticity generation in the RFD region is a crucial aspect of the intensification of near-ground rotation.

Although identifying robust kinematic differences between tornadic and nontornadic mesocyclones has been a challenge, in situ measurements during and since VORTEX1 (Markowski et al. 2002; Shabbott and Markowski 2006; Grzych et al. 2007; Hirth et al. 2008) of outflow temperature within supercells have revealed that tornadogenesis likelihood increases with the buoyancy of the outflow. Outflow is typically negatively buoyant; therefore, it tends to be less negatively buoyant in tornadic supercells. It remains much more difficult to obtain thermodynamic observations (and microphysical observations, which strongly influence the thermodynamic characteristics of the outflow) than wind measurements, especially aloft, given that in situ thermodynamic observations are still far more reliable than those that are retrieved from a series of dual-Doppler-based, three-dimensional wind syntheses. The identification of recurring kinematic differences between nontornadic and tornadic mesocyclones would be welcome, given the relative ease of obtaining kinematic versus thermodynamic observations.

Since VORTEX1, the truck-borne Doppler On Wheels (DOW) radars (Wurman et al. 1997; Wurman 2001) have collected dual-Doppler observations of several tornadic and nontornadic low-level mesocyclones. The wavelength and the stationary, half-power beamwidth of DOW radars are 3 cm and 0.93°, respectively. The DOWs typically are deployed 5–15 km from the mesocyclone with baselines of ~10 km, affording a data spacing of ~100 m within the mesocyclone region and observations as low as 50–100 m AGL. The antenna rotation rate of up to 40° s^{-1} enables fast scanning; a volume typically comprising 12–15 elevation angles from 0.5–20° is scanned in roughly a minute within a 140–180° sector. Thus, the time and space resolution within DOW dual-Doppler networks is significantly better than that of dual-Doppler datasets typically obtained by airborne or fixed ground-based platforms.

One limitation of DOW datasets is the relatively shallow region scanned in a typical deployment very near the storm. Observations are usually confined to the lowest 2–3 km AGL—e.g., a 20° elevation angle scan is 3.6 km AGL at a range of 10 km. Moreover, the 3-cm wavelength is attenuated more rapidly than the 10-cm wavelength of a WSR-88D, with DOWs usually being positioned to the east and southeast of a supercell in order to minimize the amount of precipitation that must be penetrated. Recent high-resolution dual-Doppler analyses using DOW data have revealed considerable submesocyclone structure in supercells, such as misocyclones along the rear-flank gust front (Marquis et al. 2006; Wurman et al. 2007a,b), secondary rear-flank gust fronts located behind the leading rear-flank gust front (Wurman et al. 2007a, 2011; Marquis et al. 2008; Marquis 2010), and small-scale details in hook echoes that have contributed to the recent re-evaluation of the mechanisms by which hook echoes develop (Beck et al. 2006; Byko et al. 2009).

The purpose of this study is to present analyses of the wind fields of three nontornadic low-level mesocyclones relatively recently observed by the DOWs. The supercells occurred on 3 May 2001, 12 June 2004, and 17 June 2004. We focus on the time periods when low-level rotation was strongest [the time of *tornadogenesis failure* according to Trapp (1999)], i.e., at the time of maximum azimuthally averaged tangential wind (measurement methods described in section 3d), when the supercells most closely resembled tornadic supercells. Indeed, all three nontornadic low-level mesocyclones, as will be evident in section 3, displayed characteristics (e.g., Fig. 1) similar to tornadic low-level mesocyclones, even those that have been observed at similarly high resolution. Thus, we feel that these nontornadic cases are particularly worthy of documentation.

The observations are limited to the low-level mesocyclone regions that tend to be observed best by the DOWs, and our attention is concentrated on the closed circulation that is occluded by the rear-flank gust front. (By *occluded*, we mean that outflow from the rear flank has wrapped around the circulation center, thereby separating the circulation center from the typically warm, environmental inflow, similar to how an occluded extratropical cyclone is cutoff from the warm sector at the surface.) Although there commonly are multiple vertical vorticity maxima at low levels, particularly along the rear-flank gust front (and the maximum low-level vertical vorticity might actually be associated with one of these vorticity perturbations), our focus is on the vertical vorticity maximum associated with the circulation center and its "secluded" surroundings. The wind field resembles that of an extratropical cyclone that has a "bent-back" frontal structure and "seclusion"; e.g., Shapiro and Keyser 1990).

We do not attempt to distinguish between low-level mesocyclones and what some have identified as the *tornado cyclone* (e.g., Rasmussen and Straka 2007). The classification is subjective, and it is unclear whether there are robust dynamical distinctions between low-level mesocyclones and so-called tornado cyclones. Some investigators might identify tornado cyclones within the datasets presented herein.

This paper is motivated by the following questions:

- What are the characteristics of the wind field in nontornadic low-level mesocyclone regions (e.g., horizontal divergence, horizontal and vertical vorticity, circulation, asymmetries in the wind field with respect to the circulation centers, fine-scale structure of vortex lines)?
- What paths are taken by air parcels that pass through nontornadic low-level meso-cyclones?

- If the low-level mesocyclone region is better resolved, as with DOWs, will kinematic differences between tornadic and nontornadic mesocyclones be more apparent than in past coarser-resolution studies?

There are other dual-DOW datasets of nontornadic supercells that are not presented herein, because those storms lacked strong low-level rotation. For example, we excluded storms with little or no precipitation reaching the surface near the updraft, such that no outflow or wind perturbations (e.g., no gust fronts, no significant flow curvature or vertical vorticity) were detected at low levels beneath the midlevel updraft. Downdrafts and outflow are well-known prerequisites for tornadogenesis, at least in environments lacking significant, preexisting vertical vorticity at the surface (e.g., Davies-Jones 1982; Davies-Jones and Brooks 1993; Davies-Jones et al. 2001). Although such nontornadic supercells might pose a challenge for forecasters—they all possessed midlevel mesocyclones that would have been detected by WSR-88D—we did not view these storms as being the most useful to compare with tornadic cases because the differences in the low-level wind fields are obvious. The present paper considers nontornadic circulations that are particularly difficult to discriminate from tornadic circulations.

In section 2 we describe the datasets and analysis techniques. In section 3 we present the analyses of the storms. The analyses are followed by discussion and concluding remarks in section 4.

2. Data and analysis methods

a. Cases

The observations reported in this article were obtained from storm intercepts on 3 May 2001 (near Brownfield, TX), 12 June 2004 (near Sprague, NE), and 17 June 2004 (near Las Animas, CO). Although strong rotation was observed in each of the three low-level mesocyclones (Fig. 1b,d,f), we are reasonably comfortable in referring to the circulations as nontornadic. In past DOW studies, a 20 m s^{-1} vortex-relative tangential velocity (i.e., 40 m s^{-1} maximum inbound-outbound velocity differential) has been a threshold for defining a vortex as tornadic. The rationale is that such a tangential velocity, combined with a typical translational speed of 10 m s^{-1}, produces a peak wind speed of 30 m s^{-1}, usually sufficient to cause damage. The inbound-outbound velocity differentials observed in the three mesocyclones investigated herein were always <30 m s^{-1} at the lowest radar elevation angles, typically located ~100 m AGL at the range of the circulations. Moreover, tornadoes were not observed visually by the DOW crew during these deployments, or by other reliable storm spotters, as there are no tornado reports in *Storm Data* associated with these supercells.

1) Brownfield storm

The 3 May 2001 supercell (hereafter the Brownfield storm) developed along a dryline, in an environment containing relatively low CAPE and modest vertical wind shear. Based on the 0000 UTC (4 May) sounding at Midland, TX, CAPE was estimated to be ≈800 J kg^{-1} in the storm environment. The magnitude of the 0-6 km vector wind difference, hereafter 0–6 km shear,[2] was estimated to be ≈18 m s^{-1}. The DOWs were deployed 17.0 km apart in a west-east line to the south of the storm (Fig. 1a,b). This is a somewhat long baseline (and therefore large dual-Doppler lobe) for DOW deployments during this project, and, combined with a slow storm motion, led to an unusually long period of dual-Doppler observations. Dual-Doppler data were collected from 0103–0230 UTC (4 May). DOW2 and DOW3 collected synchronized volumes every 70 s. DOW2 (DOW3) collected 14 (12) elevation angles from 0.5–21.7° (0.5–15.7°), which sampled the storm from 0.1–4.6 km AGL (0.1–3.3 km AGL) at the range of the circulation center. In this case and in the others, our focus is on the period when low-level rotation was strongest, which we define as the time of maximum azimuthally averaged tangential wind with respect to the objectively determined center of circulation (described in section 2c) in the lowest 500 m, within a radius of 2 km. In the cases herein, this time also corresponded to maximum vertical vorticity). Low-level rotation peaked at 0159 UTC.

[2] Though the terminology *0–6 km shear* is common in forecasting, it virtually always refers to the magnitude of the vector wind difference between anemometer level (typically 10 m AGL) and 6 km AGL, as it does here.

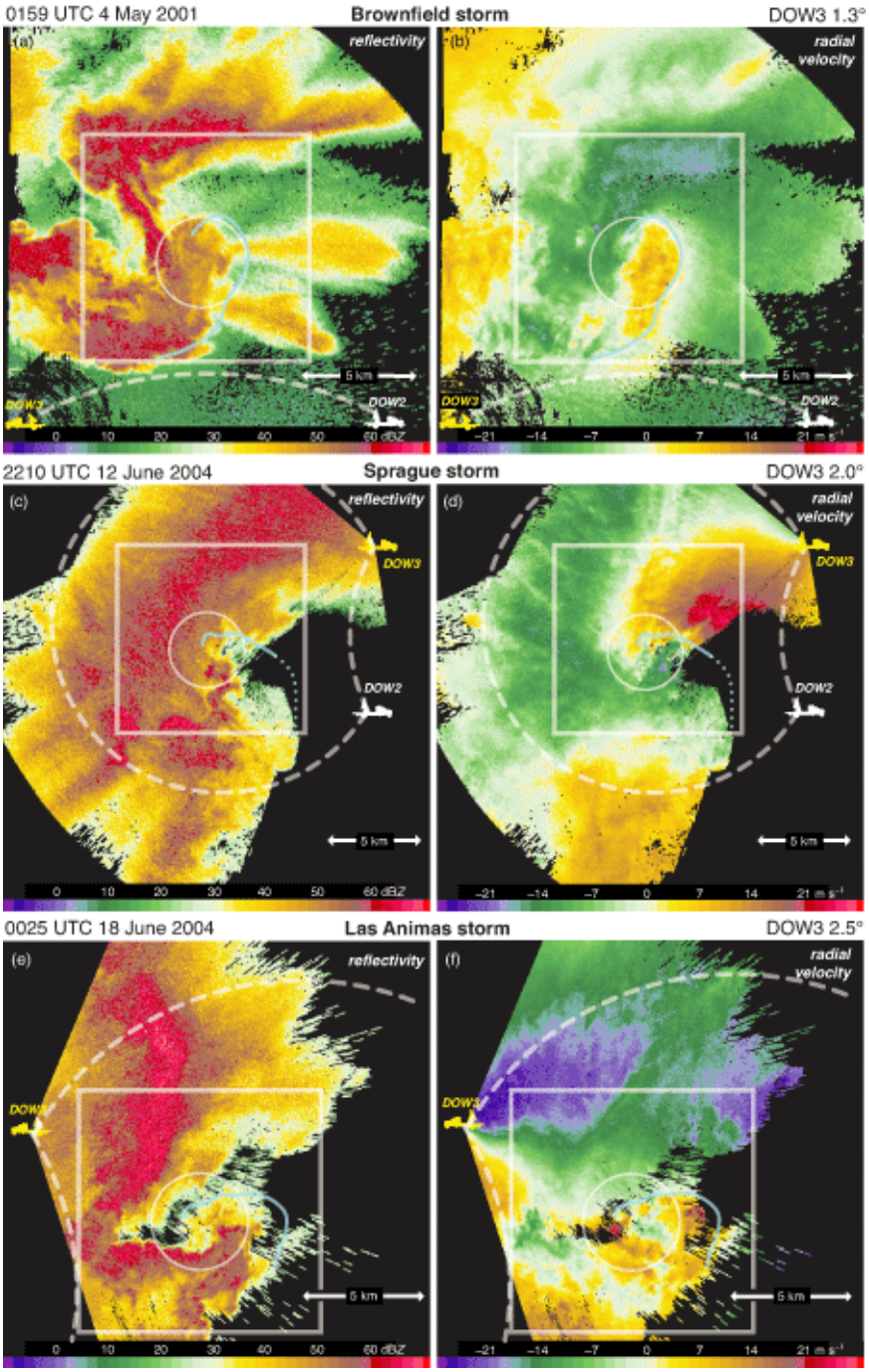

Figure 1: Logarithmic radar reflectivity factor (dBZ) and radial velocity (m s^{-1}) in the (a–b) Brownfield, (c–d) Sprague, and (e–f) Las Animas supercells, at the time of maximum low-level rotation observed by DOW3. Beams are ≈300 m AGL at the ranges of the mesocyclones. Reflectivity values are only approximate owing to the measurements being uncalibrated and different attenuation paths in each case, which also vary with time and are different between the radars in a single case. DOW2 (white) and DOW3 (yellow) positions are indicated, as is the dual-Doppler lobe (dashed curves; 30°/150° minimum/maximum interbeam angle allowed). White squares enclose the domains shown in Figs. 2–8. White circles have a radius of 2 km and are centered on the circulation centers (azimuthal averages in Figs. 11–13 were computed within these circles). Blue lines indicate the rear-flank gust fronts located via dual-Doppler wind syntheses. Dotted lines indicate the exptrapolated position of the gust front. *Click image to enlarge.*

2) Sprague storm

The 12 June 2004 supercell (hereafter the Sprague storm) developed along a quasi-stationary front, in an environment of moderate CAPE and 0–6 km shear, estimated to be approximately 2000 J kg^{-1} and 20 m s^{-1}, respectively, based on analyses by the Storm Prediction Center. The DOWs were deployed 8.4 km apart in an approximately north-south line to the east of the storm (Fig. 1c,d). Synchronized volumes were collected every 60 s. Both radars scanned 16 elevation angles from 0.5–17.3°, sampling the storm at 0.1–1.7 km AGL at the range of the circulation center (which was roughly equidistant from both radars). Dual-Doppler data were collected between 2203–2222 UTC, and low-level rotation was maximized at 2210 UTC.

3) Las Animas storm

The 17 June 2004 supercell (hereafter the Las Animas storm) was one of many storms that developed on the high plains of southeastern Colorado in a region of east-southeasterly upslope flow. CAPE and 0–6 km shear were estimated to be approximately 2000 J kg^{-1} and 25 m s^{-1}, respectively, also based on Storm Prediction Center analyses. The DOW radars were deployed 10.6 km apart along a north-south line and collected dual-Doppler data from 2351–0035 UTC. The initial scanning targeted a supercell to the west that exhibited negligible low-level rotation as it entered the western dual-Doppler lobe formed by the pair of radars. A new supercell rapidly developed farther east, between the two radars (i.e., over the baseline), during the 0005–0020 UTC period. Dual-Doppler wind syntheses of this storm's low-level mesocyclone region first became available at 0024 UTC, when it entered the eastern dual-Doppler lobe (Fig. 1e,f). Synchronized volumes were collected every 60 s. Both radars scanned 16 elevation angles from 0.5–17.4°, sampling the storm at 0.1–2.8 km AGL at the range of the circulation center (again, roughly equidistant from both radars). The maximum observed low-level rotation was at 0025 UTC. Rapid weakening of the parent storm and low-level mesocyclone occurred in the ensuing 10 min. By 0035 UTC, the low-level mesocyclone had nearly dissipated.

b. Objective analysis of radar data and synthesis of the three-dimensional wind field

The DOW data are rotated from a truck-relative reference frame to an earth-relative reference frame by aligning ground-clutter targets with known locations of towers, power poles, and houses. High-resolution aerial photographs are used to determine the precise locations of the ground targets. The earth-relative orientation is known to approximately 0.2° from this technique (Marquis et al. 2008; Marquis 2010). Prior to interpolation to a grid, the radar data are edited to remove noise and contamination from ground clutter and second-trip echoes. Aliased velocity data are dealiased.

The radar data are objectively analyzed to a Cartesian grid (18 km × 18 km × 3 km in each case) using the two-pass Barnes successive corrections method (Barnes 1964; Koch et al. 1983; Majcen et al. 2008). To account for the motion of the storm over the course of a volume, the horizontal position of each datum is corrected by the average distance traveled by the storm between the datum collection time and the central volume time. This prevents an artificial tilt with height of storm features, owing to their motion between consecutive radar sweeps. The objective analysis parameters (e.g., the grid spacing, degree of smoothing, and maximum allowable distance between an observation and grid point) are the same in each case, in order to facilitate comparisons among cases, and are determined with respect to the coarsest data spacing in the area of interest, following the recommendation of Trapp and Doswell (2000). The coarsest data spacing, d, in the low-level mesocyclone regions is ~300 m. Koch et al. (1983) recommended a grid spacing between $d/2$ and $d/3$; thus, a grid spacing of 100 m is used in the horizontal and vertical. The Barnes weight function is isotropic, and the smoothing parameter on the first pass, κ_0, is chosen based on the recommendation of Pauley and Wu (1990), who suggest a value of $(1.33d)^2 = 0.16$ km^2. On the second pass, $\kappa = 0.3\kappa_0 = 0.05$ km^2, based on the experiments of Majcen et al. (2008). A two-pass analysis has a steeper response function than that of the more commonly used one-pass analysis. The extrapolation of data to the grid points is not permitted in the objective analysis; thus, the radar data are only interpolated to the grid points that are within the data domain.

The three-dimensional wind field is synthesized using an upward integration of the anelastic mass continuity equation, with the lower boundary condition being that vertical velocity, w, vanishes there (i.e., $w = 0$ at $z = 0$). The zonal (u), meridional (v), and vertical wind

fields are adjusted iteratively until the change in $\overline{\rho}w$ (where $\overline{\rho}$ is the reference density at a given height) between iterations is <0.01 kg m^{-2} s^{-1}. The wind syntheses are converged for practical purposes at this point; changing the convergence criterion to 0.0001 kg m^{-2} s^{-1} changes the retrieved wind components only by O (10^{-4} m s^{-1})]. The wind data are extrapolated downward at this stage in order to apply the lower boundary condition, given that the lowest elevation angles scanned are 0.5°. Thus, the missing near-surface *u* and *v* wind components are set to be equal to those at the lowest level at which both radars collected data. Fortunately, the downward extrapolation is minimal because the lowest data available from both radars are usually only one grid level (100 m) above the ground. The extrapolation is only done in order to integrate the continuity equation; any extrapolated wind components are reset to "missing" after the wind synthesis has been completed.

Finally, the effect of hydrometeor fall speeds on the radial velocities is neglected because of attenuation along beams penetrating heavy precipitation, and because the DOW reflectivity factors were uncalibrated. Fall-speed errors are assumed to be small because of the relatively small antenna elevation angles used, most winds being retrieved from radial velocity scans having elevation angles less than 10°. Comparisons of wind syntheses in which fall speeds are parameterized in terms of the maximum reflectivity observed by the two radars at a grid point yield only small differences [O(10^{-2} m s^{-1}) RMSE for the wind components at 300 m AGL; O(10^{-1} m s^{-1}) RMSE in a volume extending from 100–1500 m AGL]; thus, we can be confident that the neglect of fall speeds does not change any qualitative interpretation of the results.

c. Identification of circulation centers

When a tornado is present, there is little ambiguity in defining the location of a circulation center. However, the best approach for defining the circulation center is less than obvious in the absence of a tornado, especially given the large departures from axisymmetry routinely observed at low levels in supercells—e.g., multiple cyclonic vertical vorticity maxima along the rear-flank gust front getting drawn into a broader cyclonic circulation, such as seen in high-resolution numerical simulations (e.g., Xue 2004) and observations (e.g., Marquis et al. 2006). Though it is tempting to identify the location of minimum circulation-relative wind speed as the center of rotation (after all, the winds relative to a moving vortex must vanish at the axis of rotation), the sensitivity of the identified locations of the circulation centers to the translation of the circulations is problematic. Based on our own experiences, we judge the uncertainty in storm or circulation motion to be a few meters per second, depending on which feature is tracked and its altitude. Changes in the assumed motion of this magnitude can shift the circulation center by up to a km in some cases. Therefore, we strongly favor an approach that does not depend on the motion of the circulation.

Instead of defining the circulation center to be at the location of maximum vertical vorticity, circulation centers are identified as the location of minimum (and negative) Okubo-Weiss number (Okubo 1970; Weiss 1991), that is, where vorticity dominates strain. The Okubo-Weiss number (W) is defined as $W = D^2 - \zeta^2$, where $D = \left(D_1^2 + D_2^2\right)^{1/2}$, D is the total deformation, $D_1 = \frac{\partial u}{\partial x} - \frac{\partial v}{\partial y}$ is the stretching deformation, $D_2 = \frac{\partial v}{\partial x} + \frac{\partial u}{\partial y}$ is the shearing deformation, and $\zeta = \frac{\partial v}{\partial x} - \frac{\partial u}{\partial y}$ is the vertical vorticity.[3]

Large vorticity is not the only property of a vortex, and high vorticity does not ensure that a vortex has been identified—e.g., high vorticity is found along most wind shift lines regardless of whether or not streamlines are highly curved in any reference frame. Vortices also tend to be associated with reduced deformation and low (dynamic) pressure, which are accounted for by W. Where W is negative and minimized, there should be a dynamic pressure minimum as a result of the so-called "spin" and "splat" (vorticity and deformation, respectively) contributions to dynamic pressure perturbations (Markowski and Richardson 2010, pp. 27–31). Thus, we believe that identifying circulation centers via the minimum in W is a better means of objectively defining circulation centers than by locating the maximum (minimum) vertical vorticity (circulation-relative wind speed). The

[3] The Okubo-Weiss number is similar to the Cohen and Schultz (2005) fluid-trapping diagnostic.

W field is obtained from vertical vorticity and resultant deformation fields that have been smoothed with a 3-step Leise filter (Leise 1982), which filters wavelengths <8 grid lengths (800 m herein) in order to suppress submesocyclone-scale details and to better capture the center of the mesocyclone-scale rotation (Fig. 2).

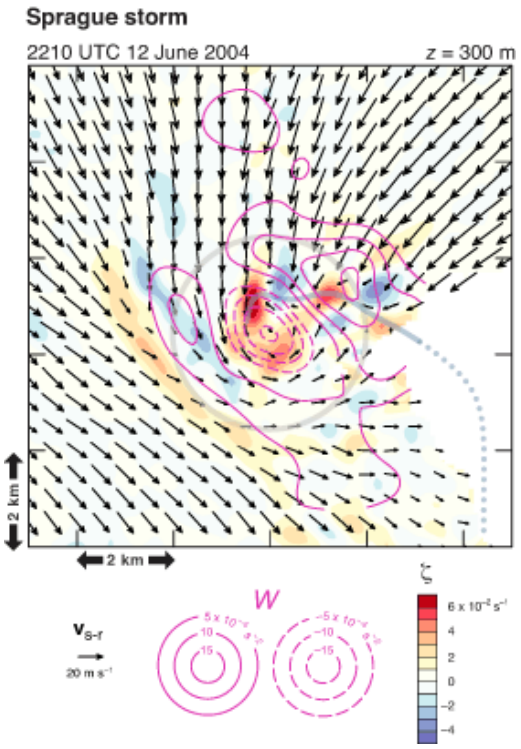

Figure 2: Vertical vorticity (ζ; shaded), storm-relative wind vectors ($\mathbf{v}_{s\text{-}r}$), and Okubo-Weiss number (*W*; magenta contours) in the Sprague storm at 300 m AGL, at 2210 UTC 12 Jun 2004. The location of thegust front is indicated (blue line, dotted where extrapolated), and a 2-km-radius circle is centered on the circulation, which is identified as the location where the *W* field (see text) is a minimum. *Click image to enlarge.*

The storm-relative reference frame is determined by tracking the circulation centers at 300 m AGL. Thus, the adjective *circulation-relative* might be more appropriate wherever *storm-relative* appears. The mean circulation motion over the 10-min period centered on *t*–0 (in the Las Animas case, the mean motion over a 5-min period from *t*–0 to *t*+5 is evaluated) is subtracted from the velocity fields shown in Figs. 2–5 and 10. The motion vectors (m s^{-1}) of the circulations in the Brownfield, Sprague, and Las Animas storms are (2.3, 1.9), (7.0, 1.0), and (2.0, –5.0), respectively.

d. Vortex line and trajectory calculations

Vortex lines and trajectory calculations are described in sections 3b and 3c, respectively. Vortex lines are computed using a fourth-order Runge-Kutta integration. The vorticity components (computed at each grid point using second-order, centered differences, except along data boundaries where one-sided differences were used) are lightly smoothed with a one-step Leise filter. This process suppresses 2Δx noise introduced by the finite differencing required to obtain the vorticity components. The qualitative characteristics of the vortex lines (e.g., whether they form arches or erupt vertically from near the ground to middle or upper levels) are fairly robust for reasonable degrees of smoothing [see the appendix in Markowski et al. (2008)].

Trajectories also are computed with a fourth-order Runge-Kutta algorithm, using a time step of 15 s (≈¼ of the time interval between wind syntheses). Time interpolation errors can affect trajectories near coherent, moving features characterized by large horizontal velocity gradients, including strong vortices. Such errors are minimized by correcting the wind velocity grids for the circulation motion prior to interpolating the grids to the time level of the trajectories. The three-dimensional wind fields are assumed to vary linearly in time between dual-Doppler analyses. The spatial interpolation is trilinear. Not surprisingly, some of the trajectories computed backward in time from the near environs of the low-level mesocyclones drop below 100 m AGL, which is the lowest grid level with wind data (recall that extrapolation was forbidden in the objective analysis, and wind components that had to be extrapolated during the wind synthesis in order to apply the lower boundary condition were flagged as missing after the syntheses were completed). To facilitate circulation analyses, we allow winds from 100 m AGL to be extrapolated to lower trajectories. The horizontal winds below 100 m AGL are assumed to equal the horizontal winds at 100 m AGL, and the vertical velocity profile is assumed to increase linearly with height from 0–100 m AGL. The degree of extrapolation is relatively minor; it occurs along <10% of the trajectories, and trajectories passing below 100 m rarely passed far lower—i.e., 95% of the extrapolated trajectories remain above 75 m AGL.

3. Nontornadic low-level mesocyclone observations

a. Characteristics of the horizontal wind field

Except where otherwise noted, the fields described in this subsection and the next are at 300 m AGL (Figs. 3–5). We chose this level in order to present the wind fields as close to the ground as possible, while limiting the fraction of the domain that fell below the radar horizons. The presentation is limited to the attributes of the fields that are vertically robust in roughly the lowest kilometer, that is, the attributes described at 300 m are evident at other levels within the 100–1000-m layer.

All three storms exhibit occluded low-level mesocyclones, in that the rear-flank gust fronts wrap around the centers of cyclonic rotation throughout the period of dual-Doppler observations (Fig. 3). The rear-flank gust fronts are analyzed subjectively along limiting streamlines. Nearly closed streamlines of the horizontal flow (in the storm-relative reference frame) encircle the circulation centers.

Sometimes, the circulation centers at 300 m AGL are displaced from those at higher altitudes by a significant distance, especially 5 min before the time of maximum low-level rotation (hereafter, "*t*–5"). For example, in the Brownfield and Sprague storms, the circulation centers at 1.5 km AGL are displaced from those at 300 m AGL by >2 km (black stars in Fig. 3a,d). The verb "displaced" is used instead of "tilted" because the circulation centers at different altitudes often cannot be associated with the same vertically coherent column of anomalously large (small) ζ (W). There is a tendency for the circulations to be most "vertically stacked" at the time of maximum low-level rotation (hereafter "*t*–0"; Fig. 3b,e,g), and in the Brownfield and Sprague storms, for the circulation center at 300 m AGL to migrate rearward relative to the circulation center at 1.5 km AGL from *t*–5 to 5 min after the time of maximum low-level rotation (hereafter "*t*+5"; Figs. 3a–c, 3d–f). The variation with height of the horizontal positions of the circulation centers will be discussed further in section 3d.

Forward-flank gust fronts (Lemon and Doswell 1979), or other wind-shift lines sometimes documented within the precipitation regions of supercells (e.g., Romine et al. 2008; see their Fig. 19), are not analyzed because of the absence of any other abrupt wind shifts, limiting streamlines, or accompanying corridors of enhanced horizontal convergence (Fig. 4). In the Brownfield storm, winds in the region ahead of the rear-flank gust front gradually back from east-southeasterly to northeasterly with increasing latitude (Fig. 3a–c). In the Sprague (Fig. 3d– f) and Las Animas storms (Fig. 3g–h), there are insufficient scatterers and/or dual-Doppler observations in the precipitation-free region east of the rear-flank gust front to identify any sharp wind shift associated with a forward-flank gust front if one might have been present there.

In some supercells, a secondary rear-flank gust front has been observed behind the primary one (Wurman et al. 2007a, 2011; Marquis et al. 2008; Marquis 2010). No such boundaries are identified in the Brownfield, Sprague, or Las Animas storms (Fig. 4), except perhaps for a brief period 5 min after the time of strongest low-level rotation in the Brownfield storm (evident as the quasilinear band of convergence behind the primary rear-flank gust front in Fig. 4c). This possible secondary rear-flank gust front has poor time continuity and no obvious translational motion.

Unfortunately, we have no reliable information about the thermodynamic characteristics of the air masses beneath the storms. The absence of an analyzed boundary does not necessarily imply the absence of significant baroclinicity, nor does the analysis of a wind-shift/convergence line imply the presence of significant baroclinicity. Attempts to retrieve the buoyancy from the radar observations produced fields that were unsuitably noisy and lacked temporal continuity.[4]

[4] Our own experiments with synthetic radar data produced by a three-dimensional numerical model, following the approach by Majcen et al. (2008), suggest that the biggest error source in the buoyancy retrievals is the estimate of the vertical perturbation pressure gradient, followed by poor estimates of the time derivatives of the wind velocity components.

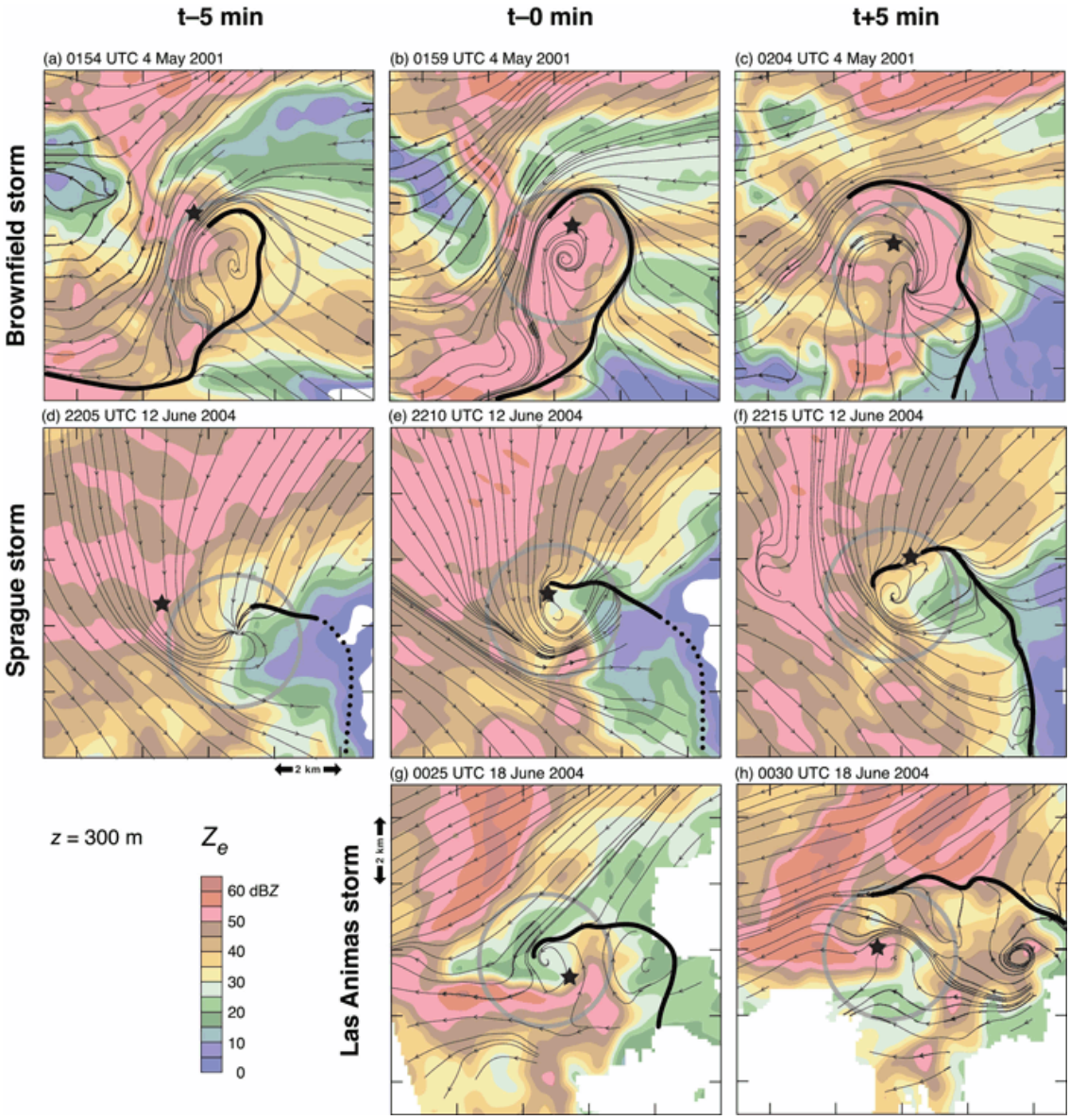

Figure 3: Objectively analyzed logarithmic reflectivity factor (dBZ) at 300 m AGL in the (a–c) Brownfield, (d–f) Sprague, and (g–h) Las Animas storms at *t*–5, *t*–0, and *t*+5 (observations were unavailable in the Las Animas storm at *t*–5). Storm-relative streamlines are overlaid, as are the rear-flank gust front locations (bold black lines, dotted where extrapolated). The gray circles have a radius of 2 km and are centered on the circulation centers (the azimuthal averages presented in Figs. 11–13 were computed within the regions enclosed by the circles). The black stars indicate the locations of the circulation centers at 1.5 km AGL. *Click image to enlarge.*

The direction of the storm-relative winds in the hook echo region varies considerably among the three storms. These wind directions might have implications for the baroclinic generation of vorticity within the hook echo, and the degree to which streamwise vorticity might be generated (Davies-Jones and Brooks 1993; Adlerman et al. 1999). In the Brownfield storm, the storm-relative winds are directed from front to rear (northeast to southwest), almost normal to the major axis of the hook echo—e.g., 3 km east and south of the northwest corner of the domain shown in Fig. 3b. In contrast, the storm-relative winds of the Sprague storm primarily are directed "down" the axis of highest reflectivity (from north to south) toward the circulation center (Fig. 3d–f). The radar echo of the Sprague storm, which was a high-precipitation

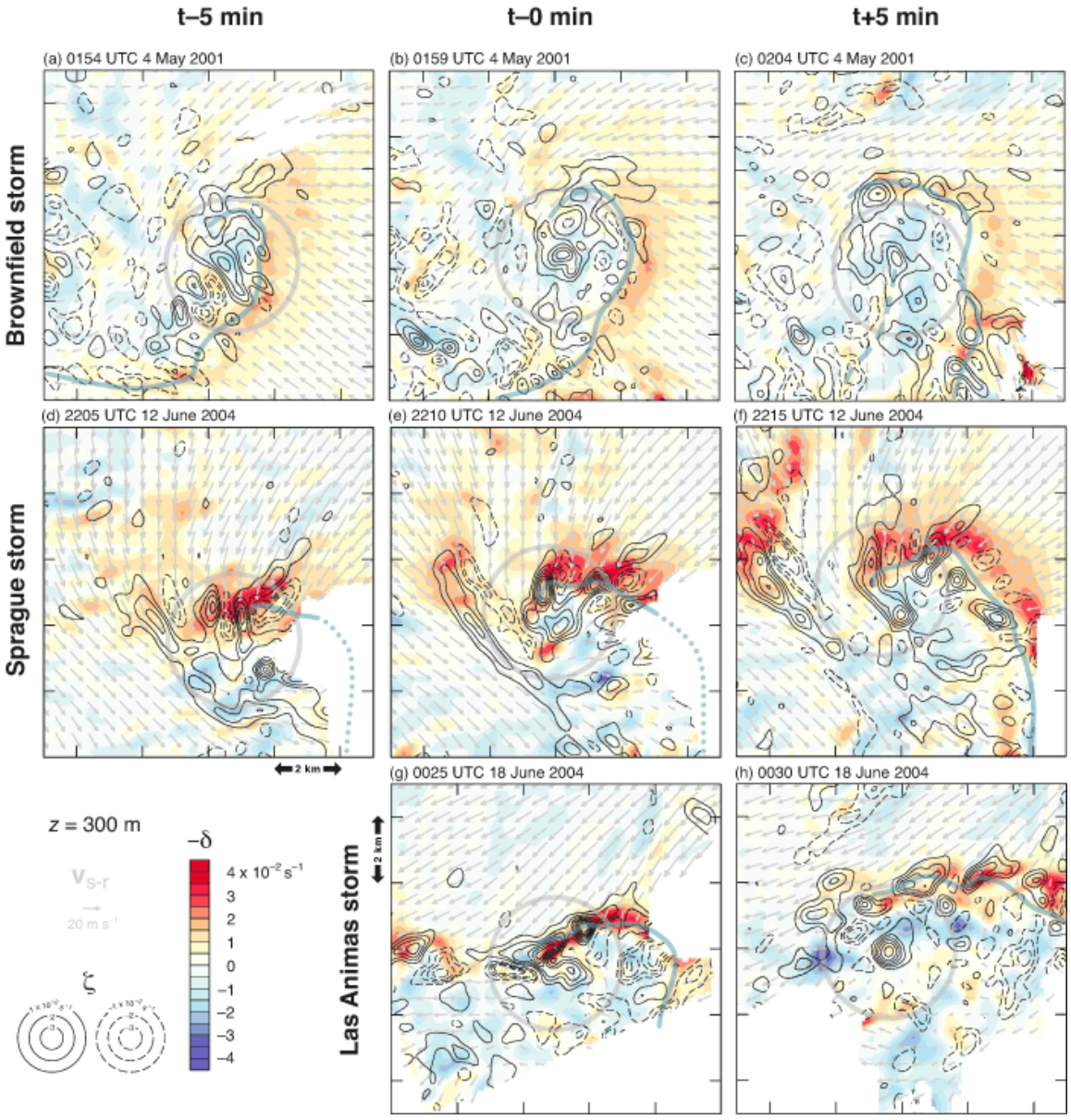

Figure 4: As in Fig. 3, but horizontal convergence (–δ; shaded), vertical vorticity (ζ; black contours), and storm-relative wind vectors ($\mathbf{v}_{s\text{-}r}$) are shown. Rear-flank gust fronts as in Fig. 2. The dashed blue line in (c) is a possible secondary rear-flank gust front. See legend for further details. *Click image to enlarge.*

supercell (Doswell and Burgess 1993), displays more of a kidney-bean appearance than a narrow reflectivity appendage. Conversely, the Las Animas storm-relative winds are directed "up" most of the long axis of the hook echo, from east to west—e.g., 3 km east and north of the southwest corner of the domain shown in Fig. 3g. At the very tip of the hook echo at *t*–0, the storm-relative wind is directed down (south to north, given that the tip of the hook echo curled northward here) the long axis of the reflectivity appendage—e.g., 4 km west and north of the southeast corner of the domain shown in Fig. 3g. In most supercell conceptual models (e.g., Lemon and Doswell 1979; Davies-Jones and Brooks 1993), storm-relative flow is directed down the hook echo. It is not known whether the observed departures from these models are related to the storms' inabilities to intensify low-level rotation to tornado strength, or whether the conceptual models themselves are deficient.

In all three storms, considerable fine-scale structure is evident in the horizontal convergence

fields (Fig. 4). There is a tendency for the horizontal convergence fields, and fields of other kinematic quantities, to be smoother in regions of inflow (i.e., ahead of the rear-flank gust front) than in regions of outflow (i.e., behind the rear-flank gust front). Brandes et al. (1988) also made this observation and argued, citing Ward (1972) and Marwitz (1972), that perturbations are damped in accelerating flows, whereas turbulence is favored in flows experiencing an adverse pressure gradient (decelerating flows). It is not clear to us, however, whether there are more perturbations in the outflow because of less damping or simply because there are more perturbations generated there.

Within a 2–km-radius ring centered on the low-level circulation, the horizontal wind field is decidedly divergent in the Brownfield storm at *t*–0 and in the ensuing 5–10-min period (Fig. 4b–c). In the Sprague storm, throughout the period of dual-Doppler observations, the same region is convergent on average (Fig. 4d–f). In the Las Animas storm, strong convergence (>0.03 s^{-1}) is present near the circulation center at *t*–0 (Fig. 4g), but the circulation center is in predominantly divergent flow 5 min later (Fig. 4h). The horizontal convergence along the rear-flank gust front is considerably stronger in the Sprague and Las Animas storms (maxima of 0.035 s^{-1}; Fig. 4d–h) than in the Brownfield storm (maximum of 0.020 s^{-1}; Fig. 4a–c).

b. Characteristics of the three-dimensional vorticity field

The vertical vorticity fields (Fig. 4) are characterized by substantial asymmetry, that is, multiple vertical vorticity maxima are evident at each analysis time, and the maximum vertical vorticity (0.05–0.06 s^{-1} at each analysis time) is not necessarily co-located with the circulation centers (e.g., Fig. 4c–g. The asymmetry is also evident in the raw radial velocity data shown in Fig. 1b,d,f. The most significant vertical vorticity maxima that are not centered on the circulation tend to be observed along the rear-flank gust front (e.g., Fig. 4c,e,g,h), as has been documented numerous times before in both observations (e.g., Marquis et al. 2006) and numerical simulations (e.g., Wicker and Wilhelmson 1995) of supercells, and believed to be attributable to horizontal shear instability. Close inspection of some analyses, however, reveals that, at some analysis times, these vorticity maxima are actually located up to 1 km behind the rear-flank gust front (e.g., Fig. 4f, immediately east of the 2–km-radius ring). We do not have an explanation for this displacement, nor can we explain the patches of anticyclonic vorticity, some with values of –0.03 s^{-1} (Fig. 4d,e) occasionally observed along the gust fronts. The small-scale vorticity extrema are unlikely to be analysis artifacts given the relatively conservative smoothing of raw radial velocity data and the fact that these extrema have good temporal continuity. Animations of the vertical vorticity field reveal that the extrema along the gust front (or just behind the gust front, as in Fig. 4f) move parallel to the gust front toward the circulation center, where they are absorbed by the vertical vorticity maximum near the circulation center. This evolution has been documented both in observations and in high-resolution numerical simulations (see references above).

The horizontal vorticity is largely streamwise 5–10 km northeast of the circulation centers in each case at all analysis times (Fig. 5), as also has been found in tornadic storms (e.g., Marquis et al. 2008; Wurman et al. 2011). In the Brownfield and Sprague storms, a large zonal gradient in the magnitude of the horizontal vorticity exists across a line extending northward from the circulation center (dashed lines in Fig. 5a–f). In the Brownfield storm, there is no low-level wind shift across this line. In the Sprague storm, the storm-relative winds only gradually shift from northeasterly to northerly from east to west across this line, and there is no prominent signature of a gust front or other air mass boundary in the horizontal convergence field along this line (Fig. 4d–f). The horizontal vorticity is weak and crosswise west of this line, and strong and streamwise east of this line in both storms.

The horizontal vorticity along and immediately behind the rear-flank gust front strongly tends to be parallel to the gust front and point toward the east or south (Fig. 5). If the horizontal vorticity in these regions is aligned with the direction of the (baroclinic) vorticity generation, then the orientation of the horizontal vorticity would imply less buoyant air behind the gust front than ahead of it. The horizontal projections of three-dimensional vortex lines, computed from a cluster of grid points centered on and near the circulation centers, and that did not extend nearly vertically and out the top of the data domain, also are roughly aligned with the

rear-flank gust front (Fig. 6). In the Brownfield and Las Animas storms, the vortex lines form arches that join regions of cyclonic and anticyclonic low-level vertical vorticity on opposite flanks of the hook echo, as also observed by Straka et al. (2007) and Markowski et al. (2008). Although many of the vortex lines originating within 500 m of the circulation centers do not form arches and simply extend quasi-vertically out the top of the domain, arching vortex lines always can be found in these cases if the vortex lines are initiated a little farther south or east of the circulation centers (especially the red vortex lines in Fig. 6). In the case of the Sprague storm (Fig. 6b), the vortex lines probably exit the data domain before they have a chance to arch back to the surface on the south side of the hook echo.

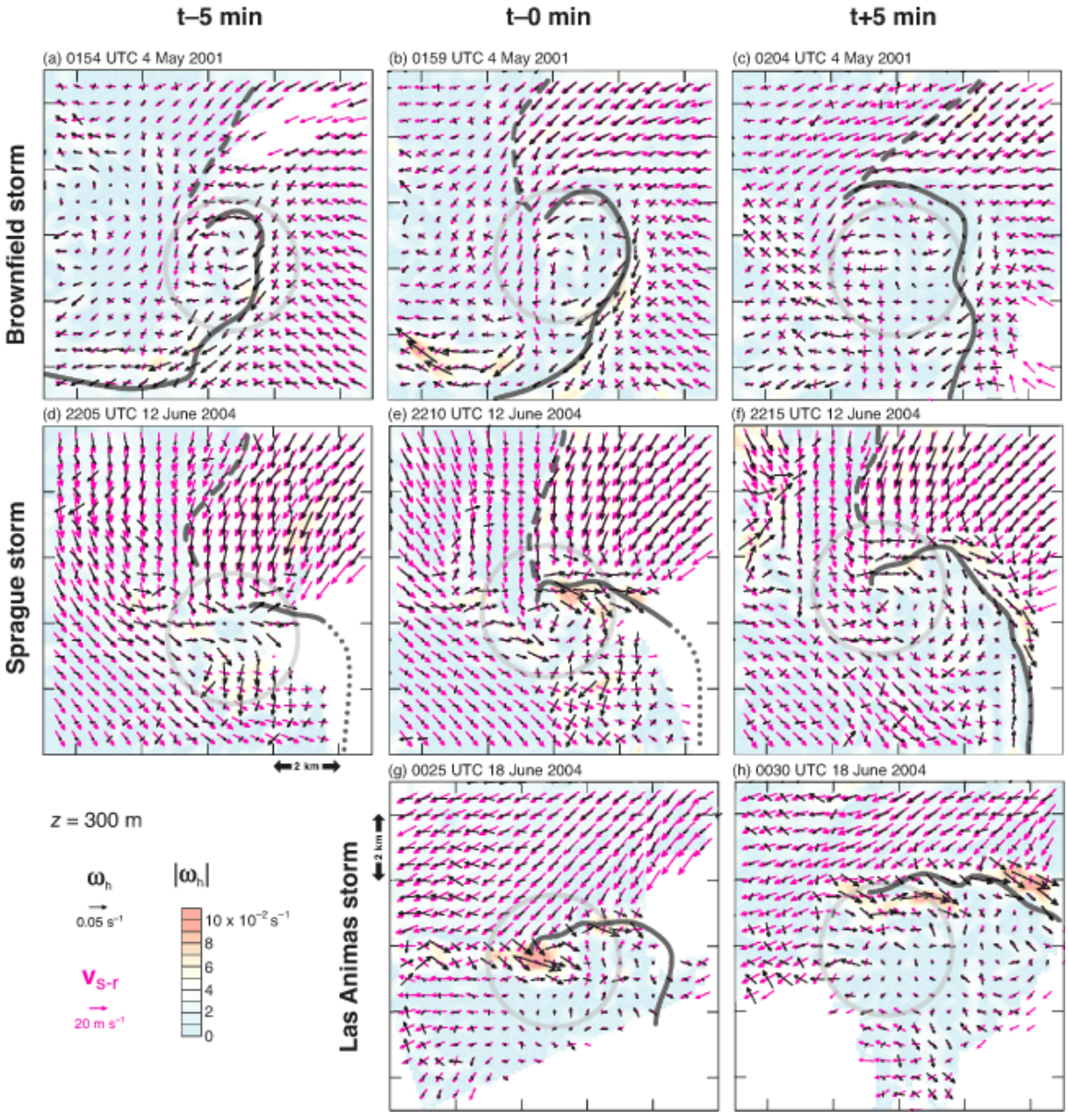

Figure 5: As in Fig. 3, but with horizontal vorticity magnitude (shaded), horizontal vorticity vectors ($\boldsymbol{\omega}_h$; black) and storm-relative wind vectors ($\mathbf{v}_{s\text{-}r}$; magenta). See legend for further details. The dashed lines in (a)–(f) identify the strong zonal gradients in horizontal vorticity magnitude described in the text. *Click image to enlarge.*

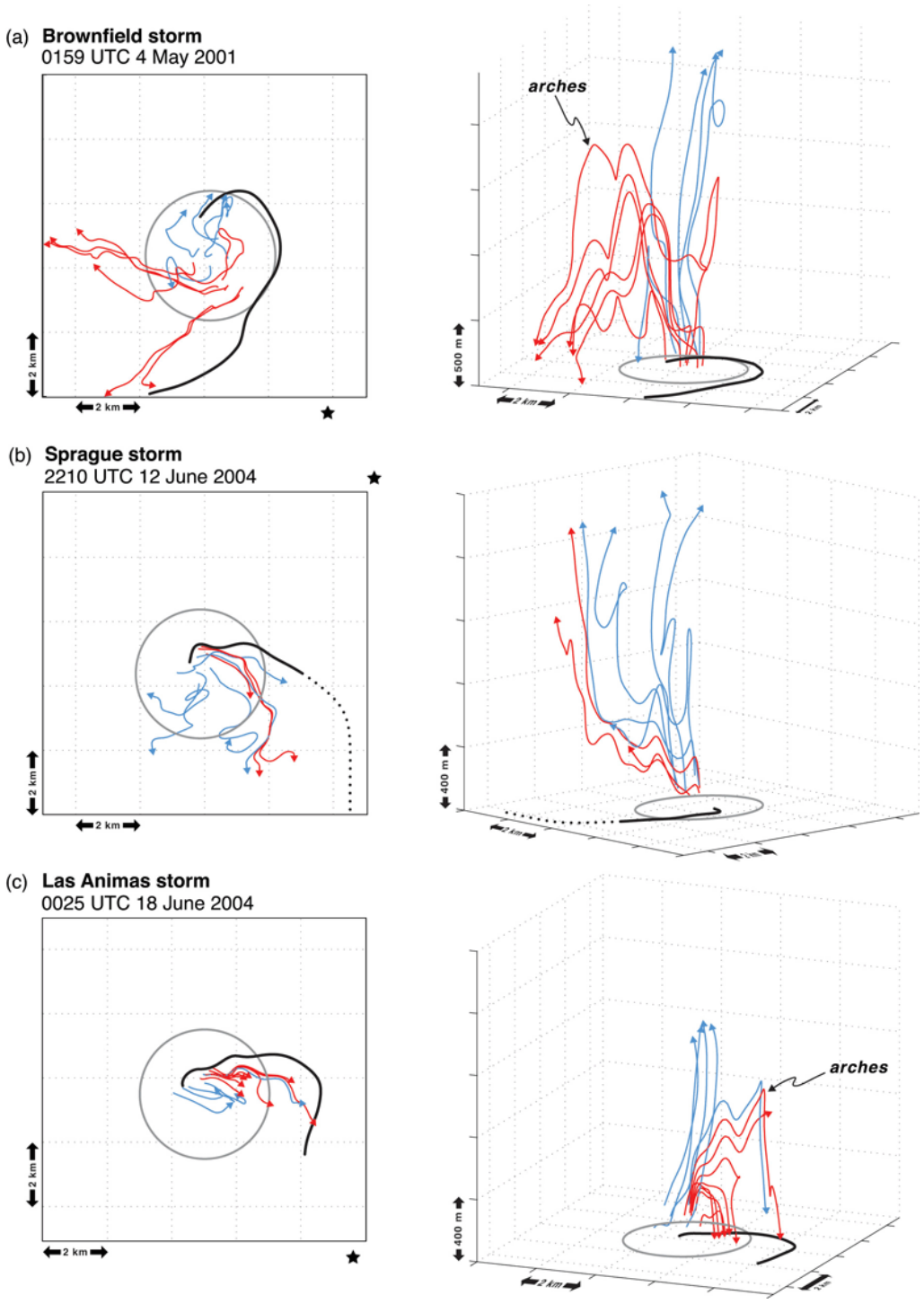

Figure 6: Vortex lines viewed from above (left) and from a three-dimensional perspective (right). The black star in each two-dimensional view indicates the approximate viewing angle in the corresponding three-dimensional panel for the (a) Brownfield, (b) Sprague, and (c) Las Animas supercells, at the time of maximum low-level rotation. The regions shown are the same as those shown in Figs. 2–5 (the same 2-km-radius circles and gust fronts are drawn in each panel). The blue vortex lines pass through the circulation centers at 300 m AGL, and 500 m north, south, east, and west of the circulation centers at 300 m AGL. The red vortex lines generally pass through points at 300 m AGL that are 750–1000 m east and southeast of the circulation centers. Vertical scale is distorted approximately sixfold. *Click image to enlarge.*

The horizontal cross-sections depicting the characteristics of the wind and vorticity fields (Figs. 3–5), as well as the vortex line characteristics described above (Fig. 6), are qualitatively similar to those in recent high-resolution dual-Doppler studies of tornadic low-level mesocyclones (e.g., Marquis et al. 2006, 2008; Wurman et al. 2007a,b, 2011; Markowski et al. 2008; Marquis 2010). That is, there are no obvious "smoking guns" in the instantaneous kinematic fields of these three nontornadic cases that distinguish them from tornadic cases. The nontornadic cases exhibit "wrapped-up" rear-flank gust fronts, arching vortex lines, and strong near-surface vortices. Recall that these three nontornadic low-level mesocyclones were chosen for analysis precisely because they so closely resembled tornadic cases. Nonetheless, it will be shown below that differences are more apparent in "higher order" calculations like trajectories (section 3c) and azimuthal (area) averages (section 3d).

c. Trajectory and circulation analyses

Two sets of trajectories are presented for each case. The first originates in a 500-m-radius ring centered on the circulation at 300 m AGL at *t*–0 (Fig. 7). For the Brownfield (Fig. 7a) and Sprague storms (Fig. 7 b), the trajectories are integrated forward and backward 5 min, thereby spanning 10 min. For the Las Animas storm (Fig. 7c), only a forward integration of trajectories over a 5-min time period is performed, given the lack of dual-Doppler wind syntheses prior to the time of maximum low-level rotation. The second set of trajectories originates in a 1–km-radius ring centered on the circulation at 300 m AGL and *t*–0 (Fig. 8). These trajectories also are integrated forward and backward in time in the Brownfield and Sprague cases, and forward in time in the Las Animas case. The circulation, $C=\oint \mathbf{v}\cdot\mathbf{dl}$ (where **v** is the three-dimensional velocity and **dl** is an element of the circuit along which the integration is performed), is computed along the 36-parcel material circuits defined by these trajectories, following the approach of Rotunno and Klemp (1985) and Davies-Jones and Brooks (1993).

The error bars in Fig. 8 indicate one standard deviation of uncertainty. Errors in circulation result from errors in the position of the circuit, as well as errors in the winds interpolated to the circuit. The uncertainty was estimated from 100 integrations of the trajectories comprising the material circuits, wherein the three-dimensional wind syntheses used to compute the trajectories were randomly perturbed in each realization. The perturbations of the *u*, *v*, and *w* wind components have a Gaussian distribution, zero mean, and standard deviations of 1 m s^{-1}, 1 m s^{-1}, and 2(*z*/1000 m) m s^{-1}, respectively. The assumed *u*, *v*, and *w* uncertainties are comparable to the uncertainties obtained in the dual-Doppler experiments using synthetic radar data performed by Majcen et al. (2008; their Table 2). Errors in the trajectories are not shown, but they are relatively small for 5-min integrations: ~50 m in *x*, *y*, and *z* based on prior error analyses by Markowski et al. (2006) and Majcen et al. (2008).

In the Brownfield storm, the air parcels within 500 m radius of the circulation center at *t*-0 spiral outward from the center and have negligible vertical excursions (Fig. 7a). In the Sprague storm, backward integration of trajectories reveals that the parcels comprising a 500-m-radius ring centered on the circulation at *t*–0 originated to the north of the center (Fig 7b). The trajectories ascend as they reach the center, but their ascent ends abruptly approximately 500 m AGL. The trajectories next descend back toward an elevation of 300 m AGL, while diverging from one another. In the Las Animas storm, trajectories also ascend close to the circulation center (Fig. 7c). The ascent is similarly halted abruptly, albeit at a higher altitude than in the Sprague storm. Trajectories reach a height of ≈1.1 km AGL, after which they descend to the lowest data level as they exit the western part of the storm.

As for the air parcels comprising a 1-km-radius ring surrounding the circulation centers at *t*–0, in the Brownfield storm, all descend in the 5 min leading up to the time of strongest rotation, some from as high as 1.4 km (Fig. 8a). The evolution of the material circuit in the Sprague storm leading up to *t*–0 is considerably different. The northern portion of the circuit originates north of the circulation center and below the circuit's elevation at the time of maximum rotation (300 m AGL); whereas the southern portion of the circuit originates south of the circulation center and slightly above the circuit's elevation at *t*–0 (parcels descend to 300 m AGL from elevations as high as 500 m AGL) (Fig. 8b).

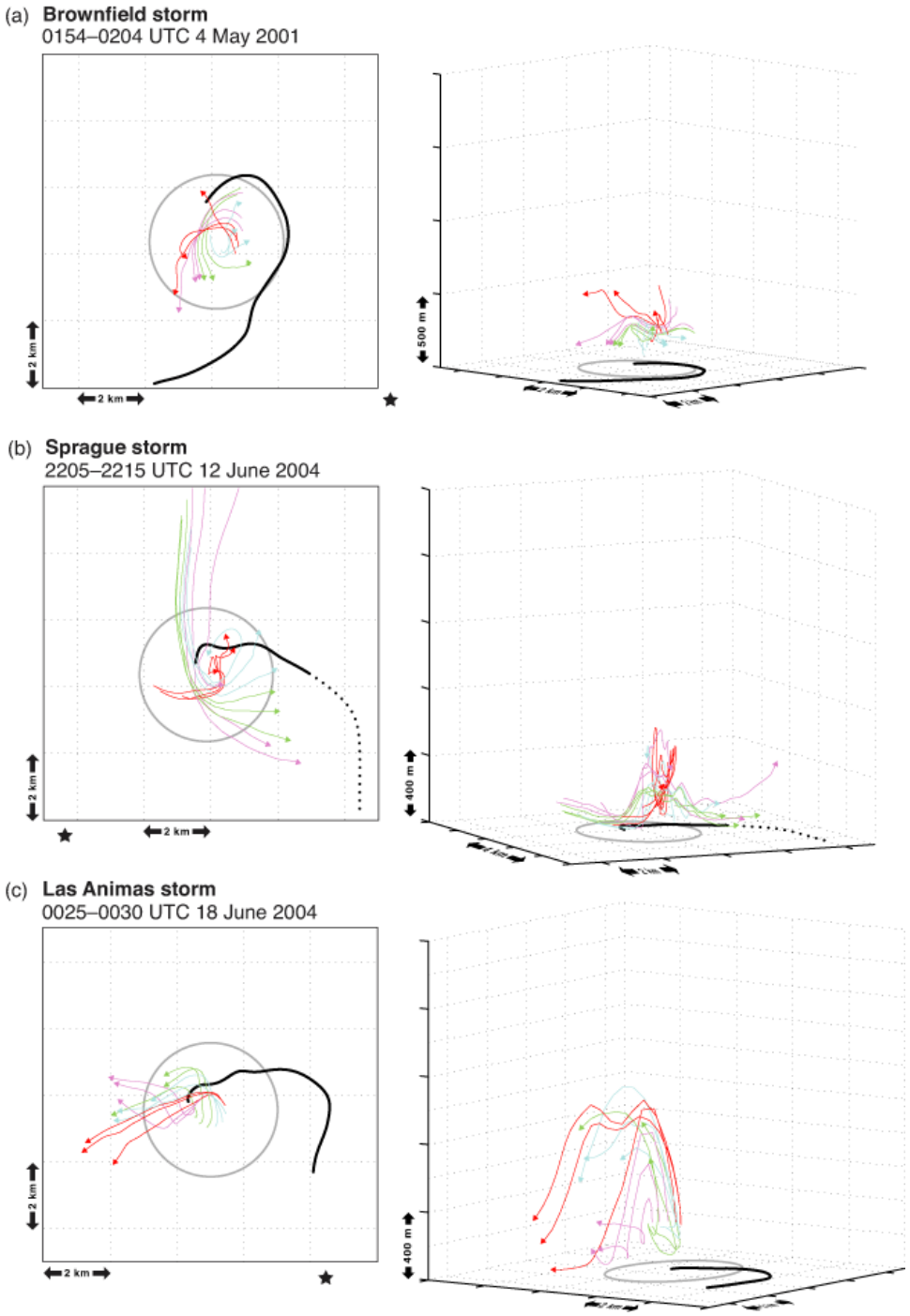

Figure 7: Trajectories viewed from above (left) and from a three-dimensional perspective (right). The black star in each two-dimensional view indicates the approximate viewing angle in the corresponding three-dimensional panel) in the (a) Brownfield, (b) Sprague, and (c) Las Animas supercells, over a 10-min period centered on the time of maximum low-level rotation. Wind syntheses for the Las Animas storm were unavailable prior to maximum low-level rotation. Regions are the same as in Figs. 2–6 (same 2-km-radius circles and gust fronts in each panel). Vertical scale is distorted approximately sixfold. The trajectories pass through a 500-m-radius ring centered on the circulation at 300 m AGL at the time of maximum low-level rotation. The red, cyan, green, and purple trajectories, respectively, pass through the northeastern, southeastern, southwestern, and northwestern quadrants of this ring at the time of maximum rotation. *Click image to enlarge.*

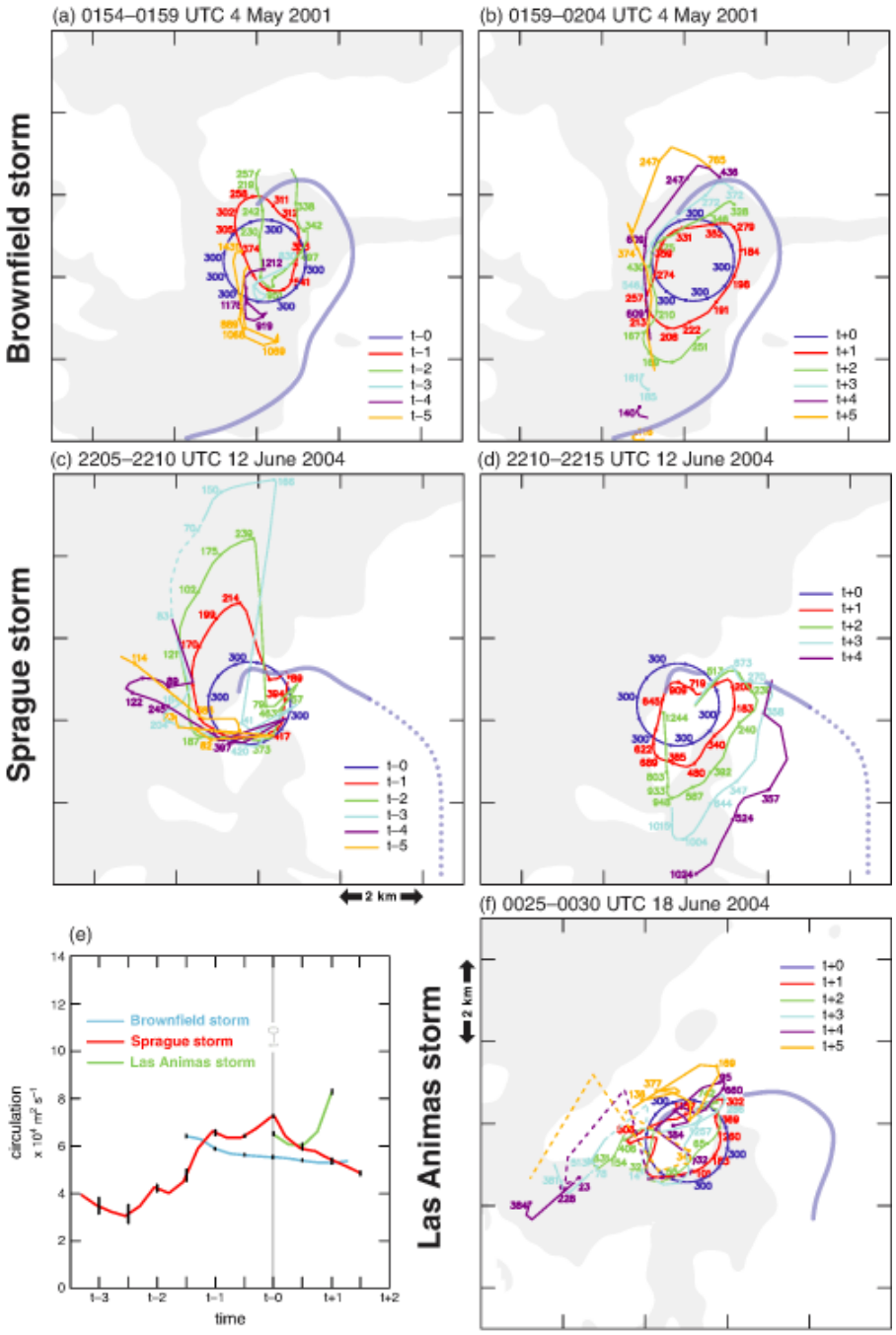

Figure 8: Horizontal projections of 36-parcel material circuits tracked 5 min (a,c) backward and (b,d,f) forward in time from the time of maximum low-level rotation (*t*–0) in the (a,b) Brownfield, (c,d) Sprague, and (f) Las Animas supercells. Las Animas wind syntheses were unavailable prior to *t*–0. The Sprague circuit could not be plotted at *t*+5 min because most of the parcels had exited the domain, and the remaining parcels were not adjacent to each other within the circuit. At *t*–0, the parcels comprise a 1-km-radius ring centered on the circulation at 300 m AGL. Numerals along the circuits indicate their heights (m AGL). Dashed lines indicate where trajectories were extrapolated below the data horizon. Gray shading indicates regions where the logarithmic radar reflectivity factor exceeds 40 dBZ at *t*–0. The rear-flank gust fronts at *t*–0 are indicated (dotted where extrapolated). In (e), the circulation about the circuits is shown as a function of time, when the circuits are entirely within the region of synthesized three-dimensional winds. Error bars (black vertical lines every 30 s) indicate one standard deviation of uncertainty. *Click image to enlarge.*

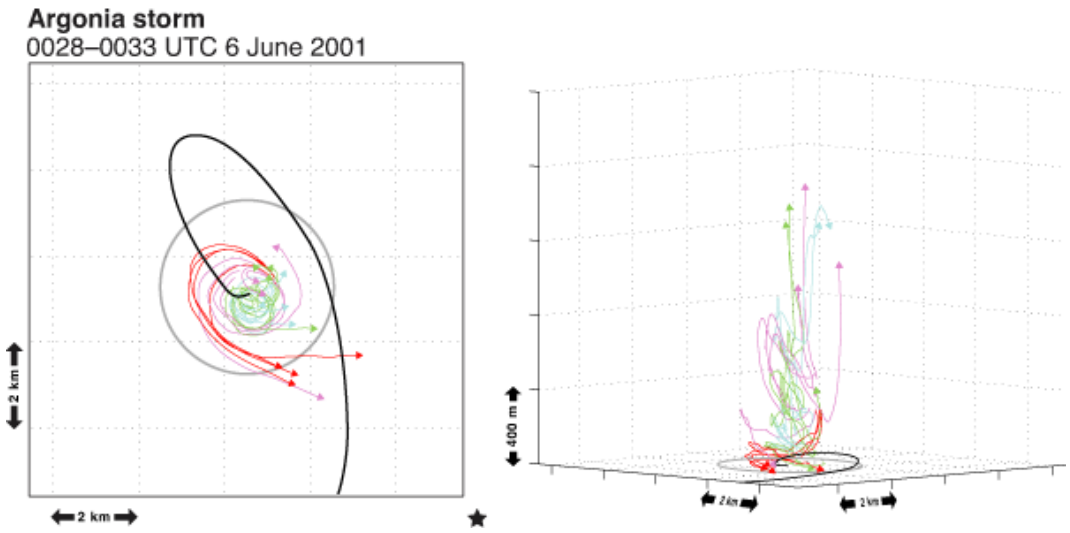

Figure 9: As in Fig. 7, but forward-integrated trajectories in the Argonia supercell, originating in a 500-m-radius ring centered on the circulation at 300 m AGL, at the approximate time of tornadogenesis. *Click image to enlarge.*

In the 5-min periods after *t*–0, the areas of the horizontal projections of the material circuits grow rapidly in the Brownfield and Sprague storms, implying mean horizontal divergence acting on the circuits (Fig. 8b,d). At least in the Sprague case, such a process is consistent with the descent also observed in the trajectories comprising the 500-m-radius ring of parcels (Fig. 7b). However, a few of the parcels comprising the material circuit exit the top of the domain (Fig. 8b,d); that is, a few "lucky" parcels have upward excursions considerably larger than those of the parcels that were located 500 m from the circulation center at *t*–0. Unfortunately, the evolution of the material circuit in the Las Animas storm is not very revealing, given the crisscrossing paths of the parcels in the circuit (Fig. 8f). Significant segments of the circuit had to be extrapolated below the data horizon after *t*+2, probably accounting for much of the (perhaps unrealistic) complexity of these circuits.

The circulation tendencies of the circuits vary considerably among the three storms. The circulation about the Brownfield circuit slowly declines in time from 6.2×10^4 m^2 s^{-1}, approximately 1.5 min prior to the time of strongest rotation, to 5.2×10^4 m^2 s^{-1} a little over a minute after the time of strongest rotation (Fig. 8e; circulation could be computed only at times when the entire circuit was within the data domain). Conversely, the circulation about the Sprague circuit nearly doubles from 3.9×10^4 m^2 s^{-1} to 7.2×10^4 m^2 s^{-1} in 3 min as the circuit is converged toward the center of rotation (Fig. 8e). Bjerknes' theorem dictates that the circulation increase only can be the result of baroclinic generation; i.e., neglecting the effects of the Coriolis acceleration and diffusion,

$$\frac{dC}{dt} = \oint B\mathbf{k}\cdot\mathbf{dl} = \oint B\,dz\,, \qquad (1)$$

where B is the buoyancy. The baroclinic generation is likely greatest along the southern portion of the circuit (south of the center of low-level rotation), because that portion of the circuit has the largest vertical projection during the period of circulation growth (Fig. 8c). Assuming $B < 0$, $dC/dt > 0$ where $\Delta z < 0$, with Δz being a finite vertical excursion of the material circuit between adjacent parcels comprising the circuit. For a given B (< 0), dC/dt increases with increasingly negative Δz. Figure 8c shows that 2–3 min before the time of maximum rotation in the Sprague storm, the southern portion of the circuit descends from >400 m AGL to <80 m AGL over a distance of less than 1 km, if tracing the circuit counterclockwise. The increase in circulation, as the circuit approaches the center of rotation, is followed by a decrease in circulation after *t*–0. Lastly, in the Las Animas storm, circulation increases abruptly during the brief 1-min evaluation period before parts of the circuit exit the data domain (Fig. 8e). The aforementioned complexity of the geometry of the circuit in this case makes it difficult to interpret the circulation trends in terms of Bjerknes' theorem.

The vertical excursions of the parcels passing through the nontornadic low-level circulations are perhaps surprisingly shallow considering those of a tornadic storm intercepted by the DOWs near Argonia, KS, on 5 June 2001 (Dowell et al. 2002). Figure 9 shows forward trajectories in the Argonia storm that originate in a 500–m-radius ring surrounding the circulation center at approximately the time of tornadogenesis[5] (0028:22 UTC 6 June). Although some trajectories abruptly descend in what might be an occlusion downdraft, many others ascend through the top of the data domain, presumably into the midlevel updraft. The degree of smoothing in the objective analyses of the radar data collected in the Argonia storm is comparable to that used in the analyses of the nontornadic cases. More will be said of the trajectory differences in section 4.

d. Azimuthally averaged fields

In this section we present vertical cross-sections (range versus height plots) of azimuthally averaged fields. The nontornadic circulation centers do not tilt much with height in the lowest 500 m, but above that, the near-ground circulations are not coupled to circulations aloft. For example, one generally cannot draw a continuous isosurface of ζ or W that would extend from the surface to midlevels (e.g., Fig. 10). (We use the term "coupled" very loosely, kinematically rather than dynamically speaking; though we easily can observe the kinematics, the presence or lack of dynamical relationships is obviously much harder to assess.) The circulation centers shift by as much as several km over just the lowest 1.5 km (Figs. 3 and 10). In some cases the shifts with height are not "well-behaved," i.e., the objectively determined circulation center jumps 1–2 km horizontally over a single grid level in the vertical as rotation aloft, presumably associated with the midlevel mesocyclone, is identified as the circulation center in lieu of the circulation center near the ground. That is, the horizontal variation of the nontornadic circulation centers with height is more complicated and severe than the tilt with height of an intense, well-defined vortex like a tornado.

Given the challenges of how best to accommodate circulation centers that shift with height in complex ways (e.g., Fig. 10) in taking azimuthal averages—challenges that ultimately stem from trying to analyze circulations in an axisymmetric framework that have considerable three-dimensional structure—we opt to keep the axis of symmetry vertical, even though the circulation center shifts a significant distance horizontally above 500 m AGL. Each axis passes through the center of circulation identified at 300 m. We believe there is value in showing the lack of vertical continuity in the vertical cross-sections in the nontornadic cases, rather than trying to track the circulation center horizontally with height in exotic ways. The latter conceals the lack of vertical continuity and makes it difficult to interpret the vertical cross-sections.[6]

Radial (V_r) and tangential (V_θ) winds about the circulation center (x_0, y_0) identified at 300 m AGL, where

$$\begin{aligned} V_r &= u\cos\theta + v\sin\theta, \\ V_\theta &= -u\sin\theta + v\cos\theta, \end{aligned} \tag{2,3}$$

and the azimuth angle $\theta = \tan^{-1}[(y-y_0)/(x-x_0)]$, were averaged azimuthally at each time. Vertical cross-sections of azimuthally averaged radial wind ($\overline{V_r}$; proportional to area-averaged divergence via Gauss' theorem), tangential wind ($\overline{V_\theta}$; proportional to area-averaged vertical vorticity via Stokes' theorem), vertical velocity ($\overline{w}$), and circulation ($C = 2\pi r\overline{V_\theta}$; r is the distance from the circulation center) are displayed for the three nontornadic cases in Figs. 11–13. The profiles are shown only for $0 \le r \le 2$ km, given the increasing asymmetry in the wind fields as the distance from the circulation centers increases, especially beyond a radius of 2 km. The regions of azimuthal averaging are indicated by the circles overlaid in Figs. 2–7.

[5] The time is approximate because of: 1) the arbitrary rotational velocity of 20 m s^{-1} used as a threshold to define a tornado, and 2) the fact that the vortex strengthened very slowly, with the rotational velocity intensifying from 15–20 m s^{-1} over a 5-min period from 0027–0032 UTC.

[6] Our choice was affected by our own experiences during the revision process. We attempted to construct cross-sections by shifting the circulation center with height, but the aforementioned complexity (sometimes requiring horizontal shifts of 1 km over a single grid level) led to vertical cross-sections that were not easily interpretable. The curious reader can find some examples in the responses to the reviewers.

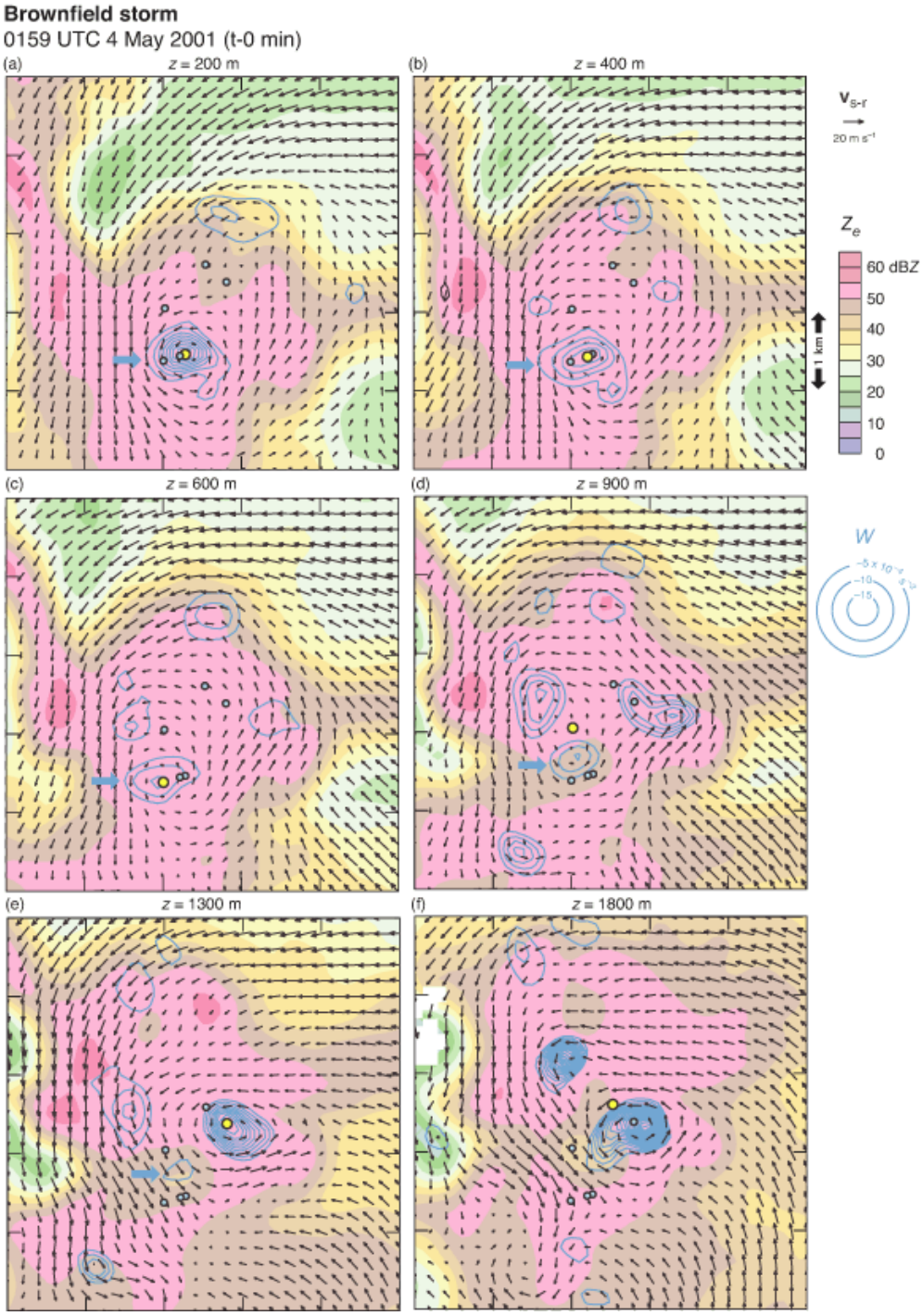

Figure 10: Unsmoothed Okubo-Weiss number (*W*; blue contours) and storm-relative wind vectors ($\mathbf{v}_{s\text{-}r}$) overlaid on the logarithmic reflectivity factor (dBZ; shaded) at (a) 200 m, (b) 400 m, (c) 600 m, (d) 900 m, (e) 1300 m, and (f) 1800 m AGL at 0159 UTC in the Brownfield storm at *t*–0 min. The yellow dot in each panel indicates the objectively identified circulation center at that level (determined using a smoothed *W* field). Green dots indicate the locations of the circulation centers identified in the other five panels. The broad blue arrow in (a)–(e) identifies the minimum in *W* associated with the near-surface circulation. This circulation weakens rapidly with height, with additional prominent *W* minima appearing above 1000 m AGL in (e) and (f). *Click image to enlarge.*

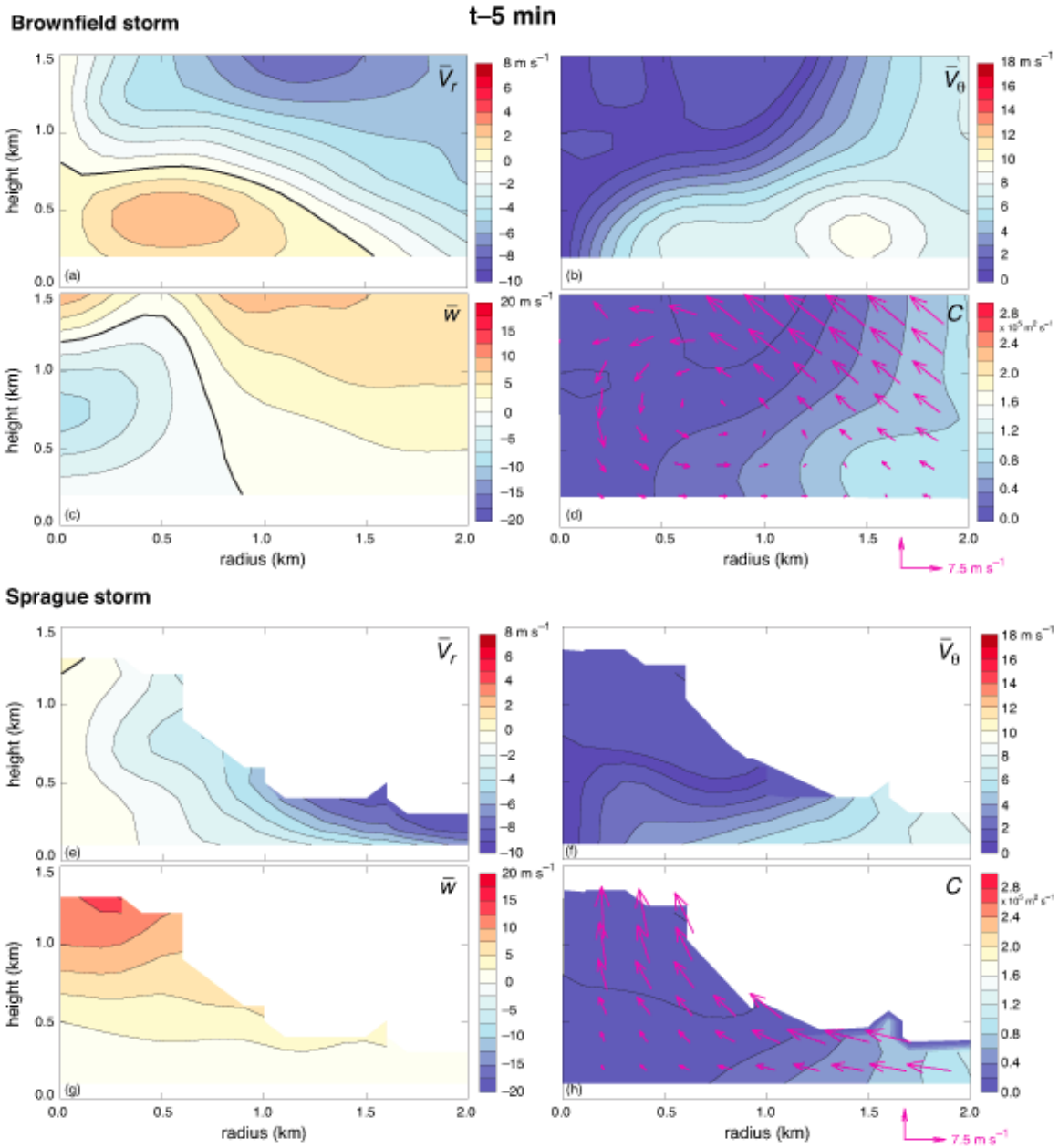

Figure 11: Vertical cross-sections of azimuthally averaged radial velocity, tangential velocity, vertical velocity, and circulation at *t*–5 min in the (a–d) Brownfield and (e–h) Sprague storms. Zero contours are emboldened. Azimuthally averaged vectors ($\overline{V_r}, \overline{w}$) are overlaid for each case atop the circulation fields. The fields were computed relative to the circulation centers at 300 m AGL. *Click image to enlarge.*

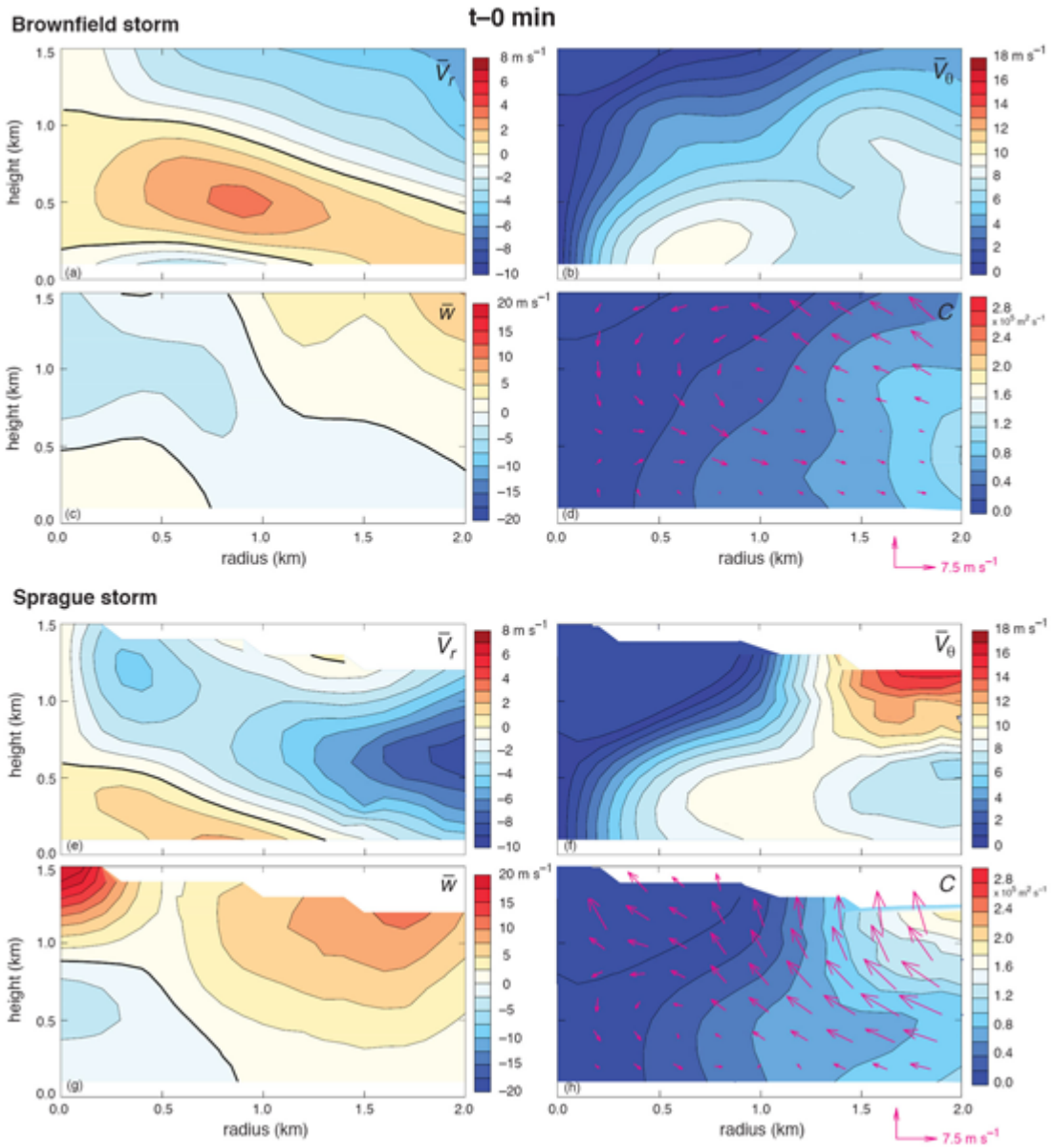

Figure 12: As in Fig. 11, but at *t*–0 min in the (a–d) Brownfield (e–h) Sprague, and (i–l) Las Animas storms. Zero contours are emboldened. *Click image to enlarge.* *(Continued on next page.)*

For comparison, azimuthally averaged fields in the Argonia storm also are presented (Figs. 14 and 15a–d), as well as azimuthally averaged fields in three other tornadic mesocyclones observed by the DOW radars (Fig. 15e–o): the Orleans storm (22 May 2004; Wurman et al. 2011), the Crowell storm (30 April 2000; Marquis et al. 2008), and the Almena storm (3 June 1999; Richardson et al. 2001). The Almena mesocyclone was associated with a strong (F3) tornado, whereas the Argonia, Crowell, and Orleans mesocyclones were associated with weak (F0–F1) tornadoes. The profiles all are derived from dual-Doppler observations (only a single level is available in the Almena case). The degree of smoothing is similar to that used for the analyses of the nontornadic mesocyclones studied herein—the Barnes smoothing parameter κ is between 0.105–0.187 km^2 on the first pass of a two-pass objective analysis, reduced to 0.3 times its initial value on the second pass. Dual-Doppler wind syntheses are available prior to

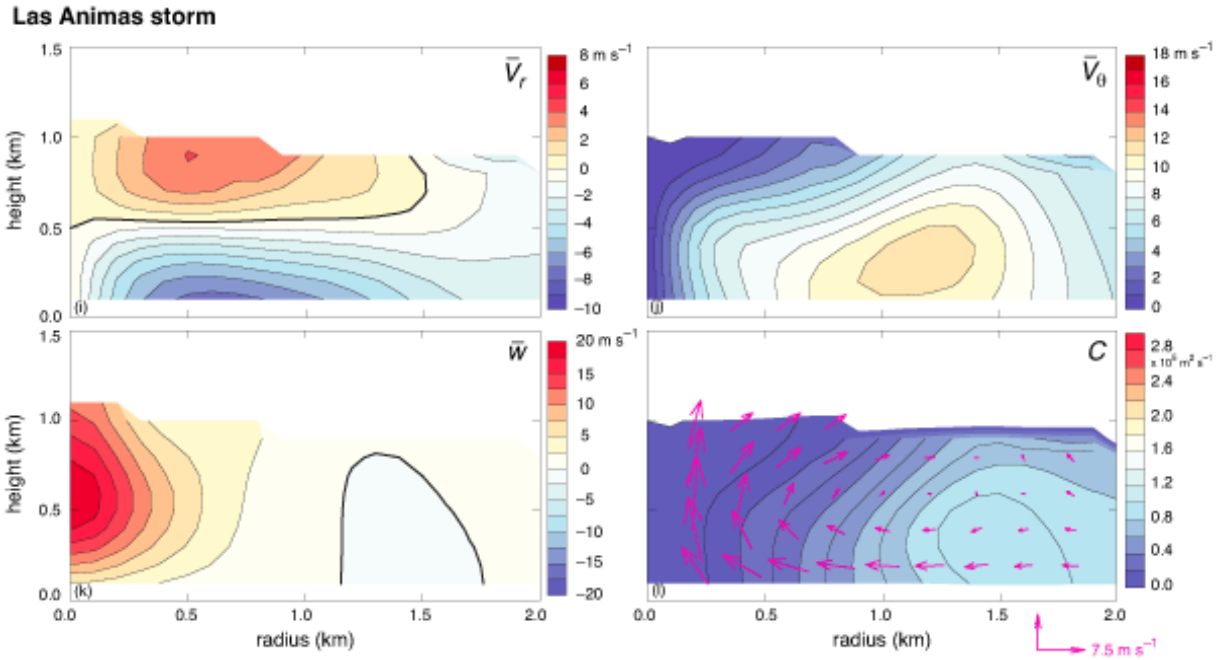

Figure 12 *(continued). Click image to enlarge.*

tornadogenesis (Fig. 14) in the Argonia case, but in the other three storms, dual-Doppler data were collected only during tornadoes (Fig. 15). The appropriateness of comparing fields during a mature tornado to fields at the time of maximum low-level mesocyclone intensity in a nontornadic storm is certainly questionable. It is perhaps better to compare the characteristics of nontornadic low-level mesocyclones, at the time of maximum low-level rotation, with those of pretornadic low-level mesocyclones; however, we have only the Argonia storm to represent dual-Doppler observation of pretornadic low-level mesocyclones.

To assess the sensitivity of the azimuthal averages to uncertainty in the chosen center location, the computations were repeated 1000 times. The circulation center was perturbed randomly, such that the standard deviation of the (x_0,y_0) coordinates was 300 m—the estimated uncertainty in the location of the circulation center, and roughly twice the data spacing. The estimated uncertainty (σ) in the $\overline{V_r}$, $\overline{V_\theta}$, $\overline{w}$, and C fields (Fig. 16) represents the mean over all of the cases of the standard deviation of the 1000 azimuthal averages computed for each case. The uncertainties in $\overline{V_r}$ and $\overline{V_\theta}$ are generally less than 1 m s^{-1}, but are larger (~1–2 m s^{-1}) in the region $400 \le r \le 700$ m (Fig. 16a,b). The uncertainty in $\overline{w}$ increases (decreases) with height (radius) (Fig. 16c). In general, $\sigma < 2$ m s^{-1}, although considerably larger uncertainty is found along the axis at relatively high elevations. The uncertainty in C increases with radius, and there is some tendency for σ to increase with height as well (Fig. 16d). For $r < 1$ km, $\sigma < 7\times10^3$ m^2 s^{-1}. There is no reason to believe that the uncertainties are associated with systematic biases that could significantly alter the general patterns observed.

At t–5, the Brownfield nontornadic circulation is characterized by radial outflow ($\overline{V_r} > 0$; Fig. 11a) and downdraft (Fig. 11c) within 750 m of the surface and 1 km of the circulation center, resulting in a down-out secondary (radius-height) circulation in that region (refer to the velocity vectors overlaid in Figs. 11d). Between t–5 and t–0, and within 1 km of the circulation center, a shallow layer of radial inflow ($\overline{V_r} < 0$ extends only to $z = 250$ m; Fig. 12a) and updraft ($\overline{w} > 0$ extends only to $z = 500$ m; Fig. 12c) develops. This results in a shallow in-up secondary circulation and the radially inward advection of circulation that gives rise to the near-surface maximum in $\overline{V_\theta}$ at t–0 (the maximum $\overline{V_\theta}$ is 9.5 m s^{-1} in the lowest 500 m; Fig. 12b). The radius of maximum $\overline{V_\theta}$ in the lowest 500 m is at r = 700 m, and is

minimized at this time.[7] By *t*+5, strong radial outflow in the lowest 1 km (Fig. 13a), downdraft (Fig. 13b), and a down-out secondary circulation (Fig. 13d) dominate the azimuthally averaged wind field. Tangential winds weaken considerably by this time (Fig. 13b), and the radius of maximum tangential wind increases to r = 1.5 km.

The evolution of the azimuthally averaged wind fields in the Sprague storm is noticeably different than the Brownfield storm. The Sprague nontornadic circulation is dominated by strong radial inflow (Fig. 11e), a strong updraft (Fig. 11g), and an in-up secondary circulation (Figs. 11h) at *t*–5. Circulation is converged toward the axis between *t*–5 and *t*–0 (cf. Figs. 11h and 12h), resulting in the maximum in $\overline{V_\theta}$ at *t*–0 (the maximum $\overline{V_\theta}$ is 9.4 m s^{-1} in the lowest 500 m; Fig. 12f). The radius of maximum $\overline{V_\theta}$ in the lowest 500 m AGL is at r = 900 m, and is a minimum at this time. But by *t*–0, the radial inflow that had been present all the way to the axis at *t*–5 is replaced by radial outflow over the lowest 500 m, and inside a radius of ~1 km (cf. Figs. 11e and 12e). Downdraft is now found in the lowest 750 m for r < 500 m where updraft previously was retrieved (cf. Figs. 11g and 12g);a down-out circulation is present within ≈750 m of the surface and axis (Fig. 12h). This is plausibly the reason for the lack of further intensification of the near-surface rotation (i.e., lack of further inward advection of C). By *t*+5, radial outflow and downdraft, albeit weak, persist near the ground for r < 500 m (Fig. 13e,g), and $\overline{V_\theta}$ has weakened accordingly (Fig. 13f).

The azimuthally averaged wind field of the Las Animas storm at *t*–0 is characterized by strong radial inflow—the strongest of all of the nontornadic low-level mesocyclones—in a 500-m deep layer extending from the axis to beyond a radius of 2 km (Fig. 12i), intense low-level updraft ($\overline{w} \approx 20$ m s^{-1} at z = 500 m along the axis; Fig. 12k), and a strong in-up circulation (Fig. 12l). The maximum $\overline{V_\theta}$ in the lowest 500 m is 11.7 m s^{-1} at a radius of 1.2 km (Fig. 12j). By *t*+5, the strong inflow stagnates (i.e., $\overline{V_r} \rightarrow 0$) at r = 500 m (Fig. 13i). A strong but much weaker updraft than at *t*–0 remains on the axis (Fig. 13k), but the near-surface secondary circulation beyond a radius of 500 m has reversed—that is, transitioned from in-up to down-out, with strong radially outward advection of circulation near the surface (Fig. 13l). Accordingly, the near-surface (z < 500 m) $\overline{V_\theta}$ field weakens considerably between *t*–0 and *t*+5 (Figs. 12j and 13j); however, strong rotation remains above the surface at an altitude as low as 500 m (Fig. 13j). The maximum in $\overline{V_\theta}$ is found at a smaller radius of r = 500 m at *t*+5.

In comparing the three nontornadic low-level mesocyclones to those associated with tornadoes, there are some notable differences. The circulation of the tornadic low-level mesocyclones (Figs. 14d and 15d,h,l,o) is much larger than that of the nontornadic mesocyclones (e.g., Fig. 12d,h,l) for r < 1 km. For example, at r = 500 m and z = 300 m, C is 2–3 times larger in the tornadic cases than in the nontornadic cases. It would be tempting to attribute these circulation differences at small radii to differences in the degree to which far-field circuits of parcels can be converged to small r, perhaps because of updraft differences that ultimately would be tied to buoyancy and/or vertical perturbation pressure gradient differences. However, even the far-field circulation tends to be smaller, by a large margin compared with the Crowell and Argonia storms, in the nontornadic versus tornadic low-level mesocyclones. For example, at r = 2 km and z = 300 m, C ranges from 0.7–1.1×10^5 m^2 s^{-1} in the nontornadic cases at *t*–0 (Fig. 12d,h,l), whereas C ranges from 1.4–2.6×10^5 m^2 s^{-1} in the Argonia, Crowell, and Almena storms at the same radius and elevation, at the times shown (Fig. 15d,l,o). The far-field circulation in the Orleans mesocyclone, however, is an exception, being comparable to that observed in the nontornadic cases (e.g., C = 0.8×10^5 m^2 s^{-1} at r = 2 km and z = 300 m; Fig. 15h). [The far-field circulation in the Almena storm (1.4×10^5 m^2 s^{-1};

[7] In prior dual-Doppler studies of mesocyclones in which azimuthally averaged fields are presented, the radar data are much coarser and more smoothing is applied in the interpolation of the data to a grid. For example, in the azimuthally averaged fields of nontornadic low-level mesocyclones presented by Trapp (1999) and Wakimoto and Cai (2000), the radius of maximum tangential wind ranges from 2–4 km (i.e., it lies *outside* of our region of azimuthal averaging) at the time of maximum low-level rotation, whereas in the cases analyzed herein, the radius is typically ~1 km.

Fig. 15o) is arguably not *substantially* larger than in the nontornadic cases, which is noteworthy given the F3 rating of the Almena tornado.]

Perhaps surprising is the comparison of the Sprague and Brownfield azimuthally averaged fields to those of the Argonia storm at *t*–5. The azimuthally averaged updraft of the Argonia storm is weaker than the azimuthally averaged updraft of the Brownfield and Sprague storms at practically all locations in the vertical cross-section (i.e., $r < 2$ km, $z < 1.5$ km) (cf. Figs. 11c, 11g, and 14c). The maximum azimuthally averaged vertical vorticity stretching (not shown), however, is larger in the Argonia storm than in the Sprague and Brownfield storms, owing to the considerably larger $\overline{V_\theta}$ and C in the Argonia storm (cf. Figs 11b,d, 11f,h, and 14b,d). Nonetheless, we believe that it would not be obvious from a casual inspection of the $\overline{V_r}$ and $\overline{w}$ fields that the Brownfield and Sprague low-level mesocyclones would be much less "tornado prone" than the Argonia low-level mesocyclone.

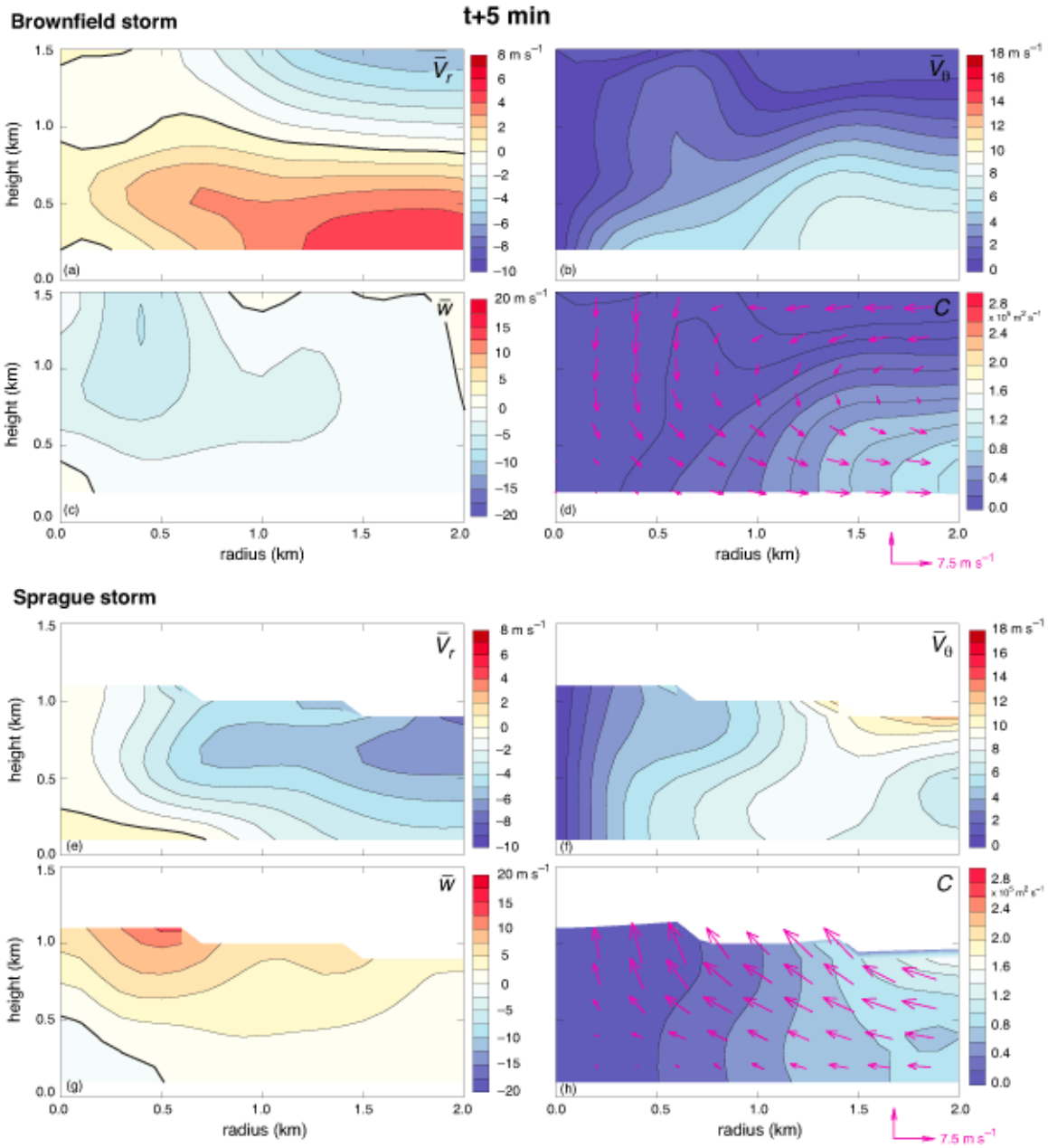

Figure 13: As in Fig. 12, but at *t*+5 min. *Click image to enlarge. (Continued on next page.)*

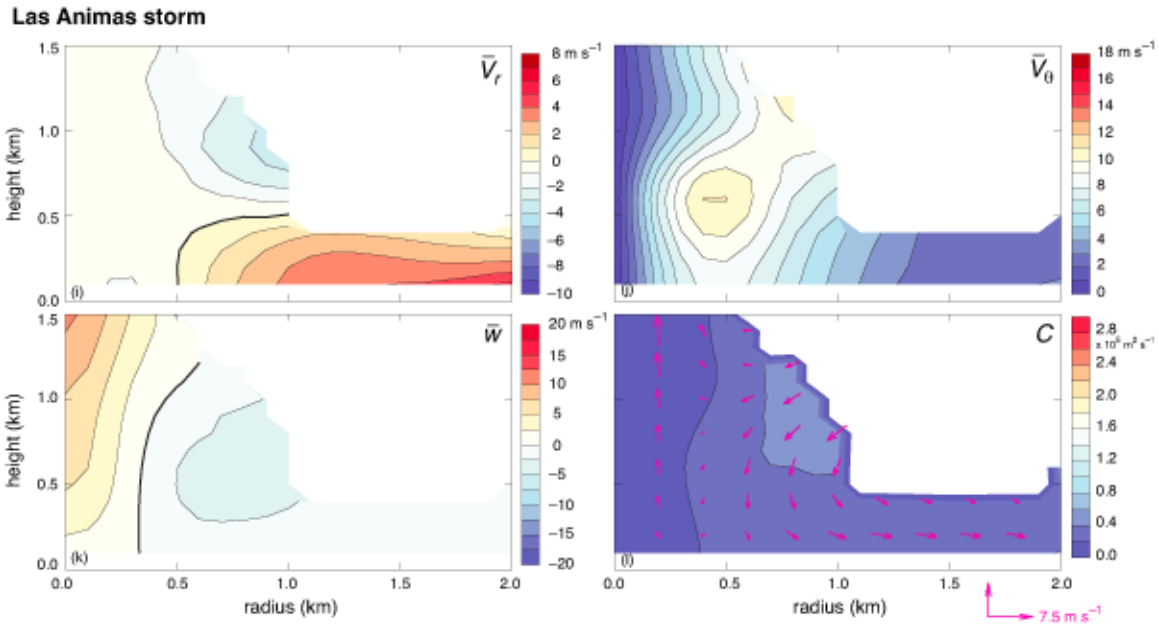

Figure 13 (continued). Click image to enlarge.

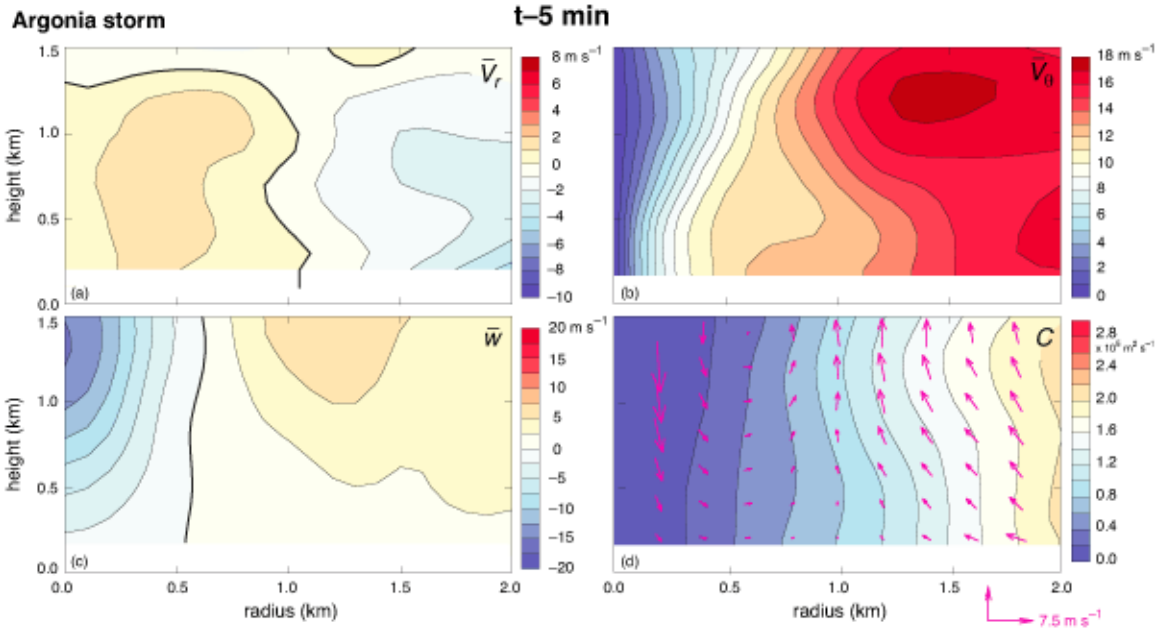

Figure 14: As in Fig. 11, but for the Argonia storm ≈5 min before the circulation reached tornadic intensity (0025 UTC 6 Jun 2001). *Click image to enlarge.*

There might well be important differences in three dimensions that are lost in the azimuthal averaging (e.g., trajectory differences noted in section 3c; cf. Figs. 7a,b and 9). Or perhaps the fact that the $\overline{V_r}$ and $\overline{w}$ fields did not seem to be decidedly more favorable in the Argonia mesocyclone at *t*–5 merely testifies to the larger circulation of the Argonia mesocyclone being the deciding factor in the vortex ultimately reaching tornado strength. Again, the Argonia tornado was relatively weak (the unsmoothed, single-Doppler inbound-outbound velocity differential was only 50 m s^{-1} at the time of maximum intensity). The Brownfield and Sprague nontornadic circulations were studied because they were notably strong; thus, there might not be a reason to anticipate substantial kinematic differences among the storms.

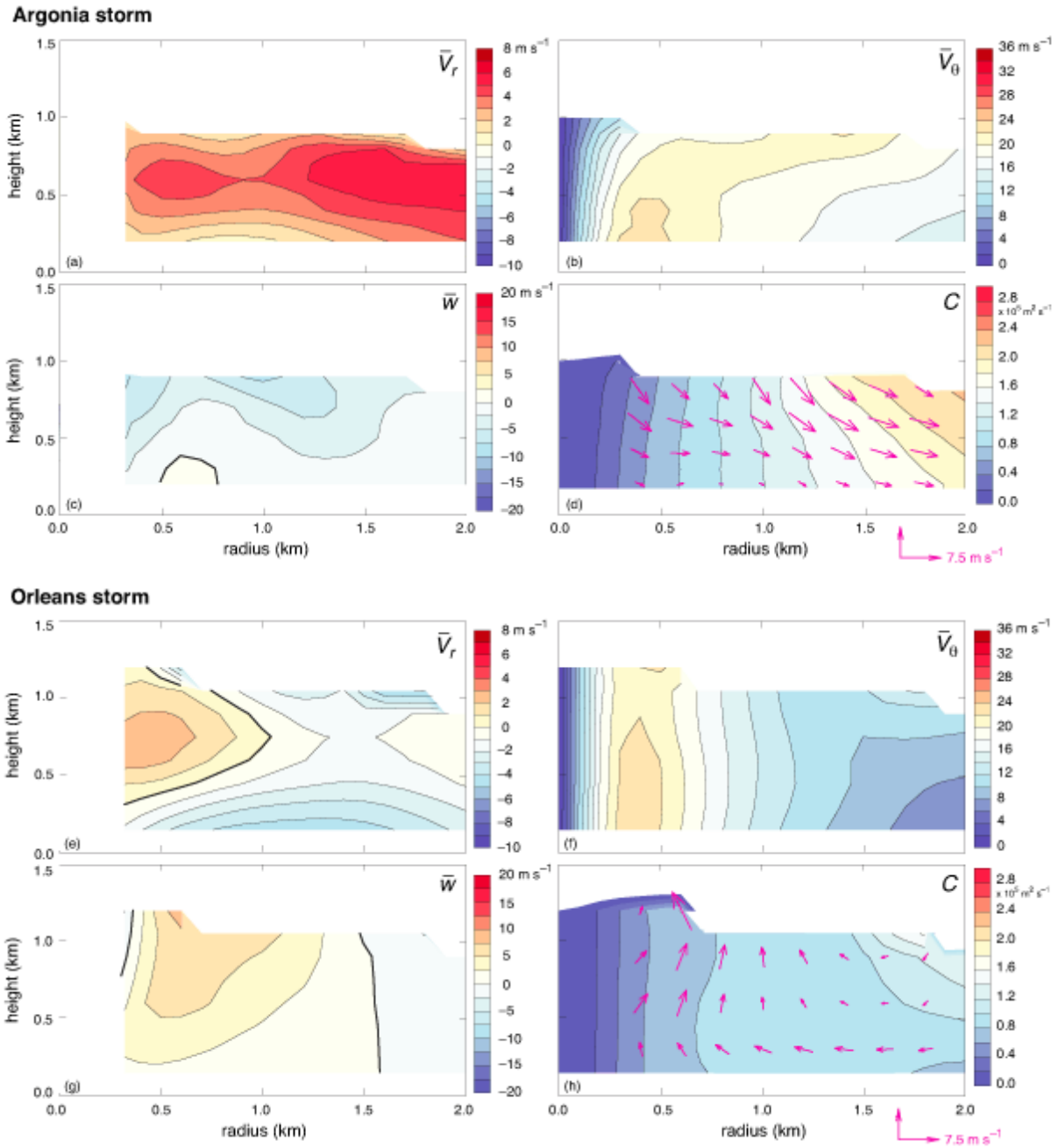

Figure 15: As in Fig. 11, but for while tornadoes were observed in the (a–d) Argonia (0033 6 June 2001), (e–h) Orleans (2304 UTC 22 May 2004), (i–l) Crowell (2112 UTC 30 Apr 2000), and (m–o) Almena (0040 UTC 4 Jun 1999) storms. The range of the tangential velocity scale is twice that of Figs. 12–15. Radial velocities and wind vectors are not shown within 300 m of the axis of rotation owing to large contamination of the radial velocity by hydrometeor centrifuging (Dowell et al. 2005). Winds were only available at a single level (175 m AGL) in the Almena case; thus, vertical velocities and vectors could not be obtained. *(Continued on next page.)* *Click image to enlarge.*

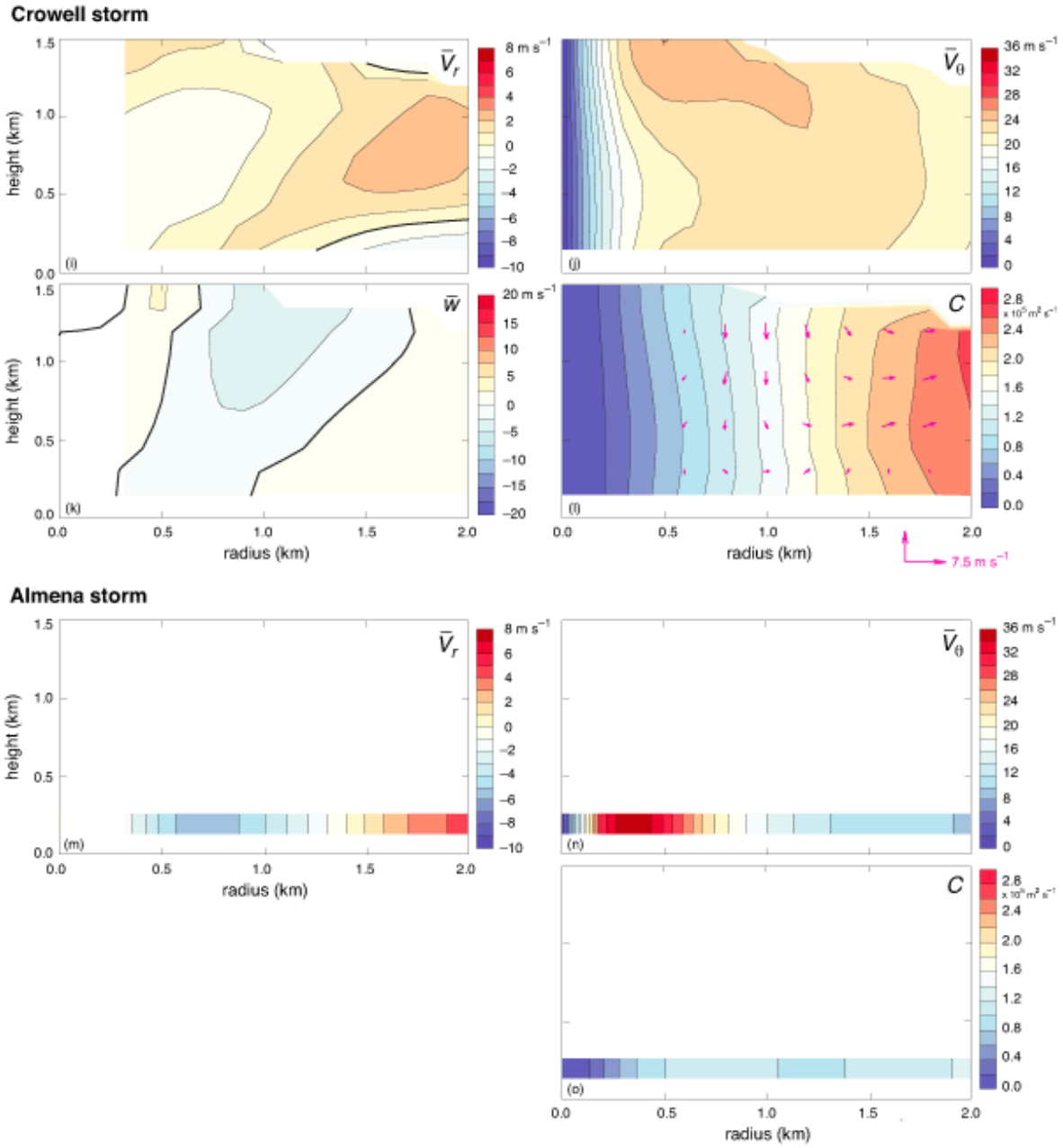

Figure 15 *(continued). Click image to enlarge.*

Comparisons between the azimuthally averaged kinematic fields of the nontornadic and tornadic low-level mesocyclones also indicate a relative shallowness of the nontornadic circulations in the vertical cross-sections, which, as described earlier in the subsection, is best interpreted as a shortcoming in the vertical continuity of the nontornadic mesocyclones, given that the azimuthal averages were computed with respect to a vertical axis. For example, $\overline{V_\theta}$ decreases rapidly with height above z = 500 m at the radius of maximum winds in all three nontornadic cases (e.g., Fig. 12b,f,j). In the tornadic cases, however, there is much better vertical continuity (Fig. 15b,f,j), and in the case of the Argonia storm, this is true even in its pretornadic phase (Fig. 14b). The difference in the depths of the circulations, or degree by which the circulation centers shift horizontally with height, is perhaps not a surprising finding, given the trajectory differences described in section 3c (i.e., the trajectories passing through nontornadic low-level mesocyclones had much shallower vertical excursions than with the Argonia low-

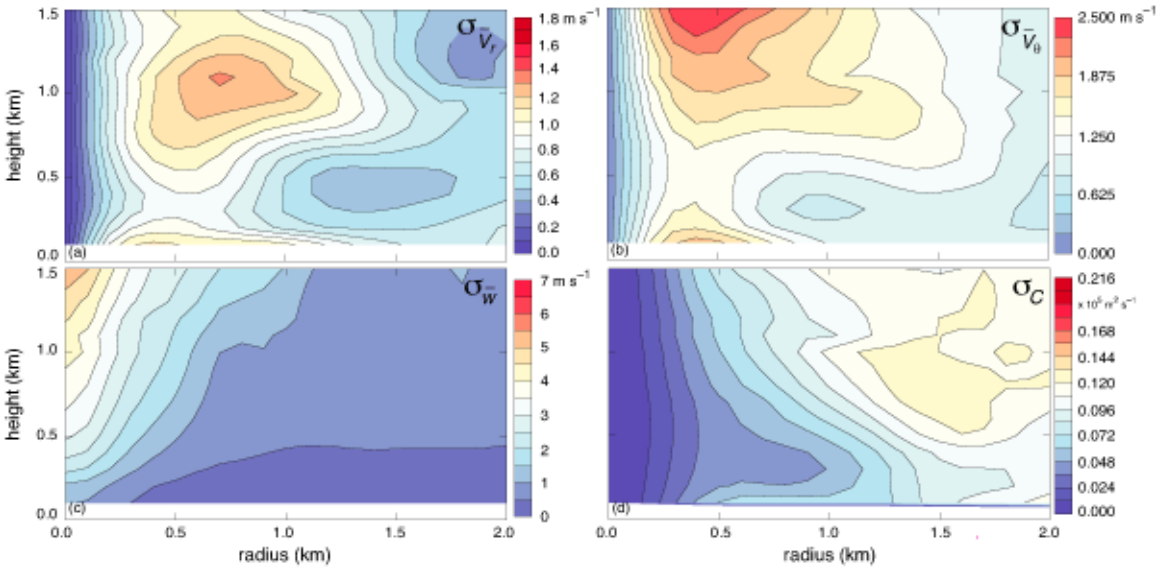

Figure 16: Estimated uncertainties (σ) of azimuthally averaged (a) radial velocity, (b) tangential velocity, (c) vertical velocity, (d) and circulation. Uncertainty estimates are determined as described in section 3d. *Click image to enlarge.*

level mesocyclone as the vortex was intensifying to tornado strength; cf. Figs. 7 and 9).

Finally, although the $\overline{V_r}$, $\overline{V_\theta}$, and $\overline{w}$ fields for the ongoing tornado cases also appear in Fig. 15 (comparisons to the *C* fields already have been made above), we do not wish to elaborate on the evolution of these fields (particularly the $\overline{V_r}$ and $\overline{w}$ fields; the $\overline{V_\theta}$ field obviously will be very different from that of a nontornadic storm when a mature tornado is in progress), other than to say that both down-out (Fig. 15d,l) and in-up secondary circulations (Fig. 15h) are observed, depending on the stage of tornado evolution, similar to observations by Rasmussen and Straka (2007). That is, the direction of the secondary circulation of a low-level mesocyclone containing a mature tornado, depending on the analysis time with respect to the evolutionary stage of the tornado, may not differ from the direction of the secondary circulation of a nontornadic low-level mesocyclone, despite the former containing a much more intense vortex. The maintenance, evolution, and demise of tornadoes and their parent circulations are beyond the scope of this study, but will be the subject of a forthcoming paper led by one of the authors (Marquis et al. 2011).

4. Discussion and concluding remarks

Many aspects of the kinematic fields of the three nontornadic mesocyclones were presented in section 3. It is challenging to know, a priori, what aspects of the mesocyclones might be important to document so that comparisons can be made to tornadic and nontornadic mesocyclone observations collected in the future. Establishing why a mesocyclone might have been nontornadic is a bit like establishing why a healthy person does not have a certain disease.

The three nontornadic mesocyclones resist generalizations. A number of differences among just these three storms were identified in section 3. What we believe to be the most noteworthy findings are itemized below.

a. Trajectories

Past observations and numerical simulations have shown that the trajectories that enter the near-surface circulation originate in the outflow (i.e., air with a history of descent). This is consistent with the findings that the rear-flank gust front tends to be wrapped around the circulation center by the time significant rotation is observed at the surface [see Markowski (2002) and references therein], as also has been observed in the storms documented herein. One might assume that these parcels would have to be able to "participate" in the parent updraft of the storm if tornadogenesis can occur. This is the case in numerical simulations in which strong vortices form at the surface (e.g., Markowski et al. 2003, 2010; Xue 2004). There is some

observational support for this idea as well, at least once a tornado has formed, e.g., the trajectories in the Argonia storm shown in Fig. 9, as well as with the numerous reports of light debris like cancelled checks being deposited many tens of miles downstream of tornadoes.

We are intrigued by the fact that trajectories passing through the nontornadic circulation centers generally rise only a few hundred meters and then abruptly decelerate, such that their ascent is halted (Fig. 7), implying that the parcels are negatively buoyant and/or the vertical perturbation pressure gradient force is insufficiently strong (or even adverse). There is no evidence that parcels passing through these nontornadic mesocyclones attained their level of free convection, if the parcels even had one. Trapp (1999) observed a decrease in the correlation between low-level vertical vorticity and vertical velocity in three nontornadic mesocyclones observed during VORTEX1 in the 5 min leading up to the time of tornadogenesis failure—i.e., the time of maximum low-level rotation. According to Trapp, "this is indicative of decoupling between low-level updraft and mesocyclone, and thus a cessation or disruption of vortex stretching." The trajectories observed herein might manifest such decoupling. The trajectories also resemble those in the idealized simulations of Markowski et al. (2010), which contained a strong cold pool. Trajectories originating in the cold pool failed to rise to midlevels (i.e., cold-pool parcels did not participate in the main updraft), and a strong near-surface vortex failed to form.

b. Circulation

Low-level circulation in the nontornadic mesocyclones was generally weaker relative to tornadic mesocyclones observed in similar detail by the DOW radars, even in the far field (i.e., several kilometers from the axis of rotation). The circulation was 2–3 times larger in the tornadic low-level mesocyclones at a radius of 500 m than in the nontornadic low-level mesocyclones. At a radius of 2 km, the circulation of the Argonia, Almena and Crowell low-level mesocyclones was roughly twice as large as that of the nontornadic cases (cf. Figs. 12d,h,l and 15d,l,o).

What processes were responsible for the extremely large circulation in some of the tornadic cases? Was it unusually large environmental horizontal vorticity, and/or environmental horizontal vorticity of a favorable orientation, converted to vertical vorticity and brought to the surface in a downdraft? Was it unusually large baroclinic generation of horizontal vorticity, and subsequent reorientation and advection toward the surface? We still do not have a thorough understanding of the dependence of the low-level circulation available for tornadogenesis on the environmental horizontal vorticity and baroclinic vorticity generation within the storm. Also, at large radii (>1 km), the nontornadic mesocyclones had circulation comparable to that in the tornadic Orleans storm. This observation suggests that the nontornadic mesocyclones had enough circulation at low levels to be tornadic, if air parcels could have converged to a sufficiently small radius. Obviously, in the absence of surface drag, conservation of angular momentum implies that large tangential velocities will be attained even by parcels having small circulation, if the parcels can reach a sufficiently small radius. It is difficult to estimate the angular momentum loss to surface friction, but the Orleans case suggests that the nontornadic cases could have been tornadic if low-level convergence would have been stronger.

c. *Secondary circulations as evident in the azimuthally averaged wind fields*

Although all three nontornadic low-level mesocyclones contained at least shallow in-up circulations near the axis of rotation leading up to the time that $\overline{V_\theta}$ attained its maximum near the surface, they also all developed down-out circulations near the axis of rotation at or shortly after the time of maximum near-surface rotation (Figs. 11d–13d, 11h–13h, 12l–13l). That is, an in-up (down-out) secondary circulation tended to be associated with near-surface vortex strengthening (weakening), which is fairly intuitive. This relationship between the intensity of vortices and the direction of the secondary circulation is identical to that documented in the (2 June 1995) Dimmitt, TX, tornado cyclone by Rasmussen and Straka (2007). The circulation they referred to as the tornado cyclone—larger in scale than the tornado but smaller than the mesocyclone—had a period of strengthening with an in-up secondary circulation, followed by weakening with a down-out secondary circulation. The failure of the vortices in the Brownfield, Sprague, and Las Animas storms to attain tornado intensity plausibly could be

viewed as the result of a premature transition from an in-up to a down-out secondary circulation, at least in an azimuthally averaged sense. (Again, caution should be taken when considering the azimuthally averaged fields herein, given all of the three-dimensional complexity.) As for the causes of this transition, the development of downward vertical velocities implies negative buoyancy and/or a downward-directed, vertical perturbation pressure gradient force.

Given the sensitivity of the secondary circulation (its direction and intensity, and therefore the sign and magnitude of the azimuthally averaged radial and vertical winds) to evolutionary stage of a tornado (Fig. 15), the tornadic cases did not always display stronger azimuthally averaged low-level radial convergence and updraft than the nontornadic cases (cf. Figs. 11–15). Nontornadic low-level mesocyclone characteristics should be compared to a larger sample of tornadic cases observed several minutes *prior to* tornadogenesis rather than while tornadoes are ongoing (additional dual-Doppler datasets of pretornadic low-level mesocyclones from VORTEX2 have not yet been analyzed completely).

d. Vortex-line arches

Vortex-line arches were observed in each of the three nontornadic mesocyclone regions. The radar data had much finer resolution and were obtained closer to the ground than in the Markowski et al. (2008) datasets; a reviewer of that paper wondered whether the findings and conclusions might be altered if observations had been obtained closer to the surface. Straka et al. (2007) and Markowski et al. (2008) have argued that observations of arching vortex lines suggest a prominent role for baroclinic vorticity generation in the hook echo region of supercells. Vortex-line arches have been observed in both tornadic and nontornadic mesocyclone regions, and we still cannot refute the hypothesis that the vortex-line arches are a ubiquitous characteristic of supercell storms.

Overall there is a lot of similarity between the low-level kinematic fields of the nontornadic and tornadic mesocyclones that have been observed by the DOWs on spatial scales larger than the tornado—e.g., occluded gust front structures, closed circulations, vortex-line arches, and circulation at a large radius that is comparable to what might be found in at least some tornadic mesocyclones. Comparisons between non-tornadic mesocyclones and would-be tornadic mesocyclones prior to tornadogenesis are especially warranted. Furthermore, given the growing number of observations of extremely subtle kinematic differences between tornadic and nontornadic low-level mesocyclones, large strides in our understanding of the conditions that favor tornadic supercells likely will require datasets that include thermodynamic and perhaps micro-physics observations, such as those that have been obtained from VORTEX2. For example, in this study, thermodynamic observations would have provided insight into the behavior of the trajectories and the relative contributions of environmental versus storm-generated vorticity to the amplification of near-surface vertical vorticity. Microphysical observations might have provided some context for the observed thermodynamic properties. We eagerly await these forthcoming VORTEX2 analyses.

ACKNOWLEDGMENTS

We are grateful for the dedication and hard work of all of the crews involved with the collection of the data analyzed. We especially thank David Dowell and Karen Kosiba for providing edited radar data for the 5 June 2001 case. We also are extremely appreciative of the suggestions of the four reviewers (David Dowell, Jana Houser, Erik Rasmussen, and Jerry Straka; we single-out David Dowell for responding to additional offline inquiries regarding his review and for helping to identify historical, dual-Doppler, nontornadic cases in the literature) and the support of the National Science Foundation (NSF awards ATM-0437512, ATM-0734001, ATM-0801035, and ATM-0801041).

REFERENCES

Adlerman, E. J. and R. Davies-Jones, 1999: A numerical simulation of cyclic mesocyclogenesis. *J. Atmos. Sci*., **56**, 2045–2069.

Barnes, S. L., 1964: A technique for maximizing details in numerical weather map analysis. *J. Appl. Meteor.*, **3**, 396–409.

Beck, J. R., J. Schroeder, and J. Wurman, 2006: High-resolution dual-Doppler analyses of the 29 May 2001 Kress, Texas, cyclic supercell. *Mon. Wea. Rev*., **134**, 3125–3148.

Bluestein, H. B., and G. R. Woodall, 1990: Doppler-radar analysis of a low-precipitation severe storm. *Mon. Wea. Rev.*, **118**, 1640–1665.

——, and S. G. Gaddy, 2001: Airborne pseudo-dual-Doppler analysis of a rear-inflow jet and deep convergence zone within a supercell. *Mon. Wea. Rev*., **129**, 2270–2289.

Brandes, E. A., 1977: Flow in a severe thunderstorm observed by dual-Doppler radar. *Mon. Wea. Rev*., **105**, 113–120.

——, 1978: Mesocyclone evolution and tornadogenesis: Some observations. *Mon. Wea. Rev.*, **106**, 995–1011.

——, 1981: Finestructure of the Del City-Edmond tornadic mesocirculation. *Mon. Wea. Rev.*, **109**, 635–647.

——, 1984: Vertical vorticity generation and mesocyclone sustenance in tornadic thunderstorms: The observational evidence. *Mon. Wea. Rev*., **112**, 2253–2269.

——, R. P. Davies-Jones, and B. C. Johnson, 1988: Streamwise vorticity effects on supercell morphology and persistence. *J. Atmos. Sci*., **45**, 947–963.

Byko, Z., P. Markowski, Y. Richardson, J. Wurman, and E. Adlerman, 2009: Descending reflectivity cores in supercell thunderstorms observed by mobile radars and in a high-resolution numerical simulation. *Wea. Forecasting*, **24**, 155–186.

Burgess, D. W., V. T. Wood, and R. A. Brown, 1982: Mesocyclone evolution statistics. Preprints, *12th Conf. on Severe Local Storms*, San Antonio, TX, Amer. Meteor. Soc., 422–424.

Cohen, R. A., and D. M. Schultz, 2005: Contraction rate and its relationship to frontogenesis, the Lyapunov exponent, fluid trapping, and airstream boundaries. *Mon. Wea. Rev*., **133**, 1353–1369.

Davies-Jones, R. P., 1982: Observational and theoretical aspects of tornadogenesis. *Intense Atmospheric Vortices.* L. Bengtsson and J. Lighthill, Eds., Springer-Verlag, 175–189.

——, and H. E. Brooks, 1993: Mesocyclogenesis from a theoretical perspective. *The Tornado: Its Structure, Dynamics, Prediction, and Hazards, Geophys. Monogr*., Vol. 79, Amer. Geophys. Union, 105–114.

——, R. J. Trapp, and H. B. Bluestein, 2001: Tornadoes and tornadic storms. *Severe Convective Storms. Meteor. Monogr.*, No. 50, Amer. Meteor. Soc., 167–221.

Doswell, C. A., III, and D. W. Burgess, 1993: Tornadoes and tornadic storms: A review of conceptual models. *The Tornado: Its Structure, Dynamics, Prediction, and Hazards*, *Geophys. Monogr*., Vol. 79, Amer. Geophys. Union, 161–172.

Dowell, D. C., and H. B. Bluestein, 2002a: The 8 June 1995 McLean, Texas, storm. Part I: Observations of cyclic tornadogenesis. *Mon. Wea. Rev.*, **130**, 2626–2648.

——, and ——, 2002b: The 8 June 1995 McLean, Texas, storm. Part II: Cyclic tornado formation, maintenance, and dissipation. *Mon. Wea. Rev*., **130**, 2649–2670.

——, Y. Richardson, and J. Wurman, 2002: Observations of the formation of low-level rotation: The 5 June 2001 Sumner County, Kansas, tornado. Preprints, *21st Conf. on Severe Local Storms*, San Antonio, TX, Amer. Meteor. Soc., 12.3.

——, C. R. Alexander, J. M. Wurman, and L. J. Wicker, 2005: Centrifuging of hydrometeors and debris in tornadoes: Radar-reflectivity patterns and wind-measurement errors. *Mon. Wea. Rev.*, **133**, 1501–1524.

Grzych, M. L., B. D. Lee, and C. A. Finley, 2007: Thermodynamic analysis of supercell rear-flank downdrafts from Project ANSWERS. *Mon. Wea. Rev.*, **135**, 240–246.

Heymsfield, G. M., 1978: Kinematic and dynamic aspects of the Harrah tornadic storm analyzed from dual-Doppler radar data. *Mon. Wea. Rev*., **106**, 233–254.

Hildebrand, P. H., C. A. Walther, C. L. Frush, J. Testud, and F. Baudin, 1994: The ELDORA/ASTRAIA airborne Doppler weather radar: Goals, design, and first field tests. *Proc. IEEE*, **82**, 1873–1890.

——, W.-C. Lee, C. A. Walther, C. Frush, M. Randall, E. Loew, R. Neitzel, R. Parsons, J. Testud, F. Baudin, and A. LeCornec, 1996: The ELDORA/ASTRAIA airborne Doppler weather radar: High-resolution observations from TOGA COARE. *Bull. Amer. Meteor. Soc*., **77**, 213–232.

Hirth, B. D., J. L. Schroeder, and C. C. Weiss, 2008: Surface analysis of the rear-flank downdraft outflow in two tornadic supercells. *Mon. Wea. Rev.*, **136**, 2344–2363.

Koch, S. E., M. DesJardins, and P. J. Kocin, 1983: An interactive Barnes objective map analysis scheme for use with satellite and conventional data. *J. Clim. Appl. Meteor*., **22**, 1487–1503.

Leise, J. A., 1982: A multidimensional scale-telescoped filter and data extension package. NOAA Tech. Memo. ERL WPL-82, 19 pp. [Available from NOAA Office of Oceanic and Atmospheric Research, Silver Spring Metro Center, Bldg 3, Room 11627, Silver Spring, MD 20910.]

Lemon, L. R., and C. A. Doswell, 1979: Severe thunderstorm evolution and mesocyclone structure as related to tornadogenesis. *Mon. Wea. Rev*., **107**, 1184–1197.

Majcen, M., P. Markowski, Y. Richardson, D. Dowell, and J. Wurman, 2008: Multi-pass objective analyses of radar data. *J. Atmos. Oceanic Technol*., **25**, 1845–1858.

Markowski, P. M., 2002: Hook echoes and rear-flank downdrafts: A review. *Mon. Wea. Rev*., **130**, 852–876.

——, 2008: A comparison of the midlevel kinematic characteristics of a pair of supercell thunderstorms observed by airborne Doppler radar. *Atmos. Res*., **88**, 314–322.

——, and Y. P. Richardson, 2010: *Mesoscale Meteorology in Midlatitudes*. Wiley-Blackwell, 407 pp.

——, J. M. Straka, and E. N. Rasmussen, 2002: Direct surface thermodynamic observations within the rear-flank downdrafts of nontornadic and tornadic supercells. *Mon. Wea. Rev.*, **130**, 1692–1721.

——, C. Hannon, and E. N. Rasmussen, 2006: Observations of convection initiation "failure" from the 12 June 2002 IHOP deployment. *Mon. Wea. Rev.*, **134**, 375–405.

——, J. M. Straka, E. N. Rasmussen, R. P. Davies-Jones, Y. Richardson, and J. Trapp, 2008: Vortex lines within low-level mesocyclones obtained from pseudo-dual-Doppler radar observations. *Mon. Wea. Rev*., **136**, 3513–3535.

——, Y. Richardson, and M. Majcen, 2010: Near-surface vortexgenesis in idealized three-dimensional numerical simulations involving a heat source and a heat sink in a vertically sheared environment. Preprints, *25th Conf. on Severe Local Storms*, Denver, CO, Amer. Meteor. Soc., 15.1.

Marquis, J. M., 2010: The maintenance of tornadoes observed with high-resolution mobile Doppler radars. Ph.D. Dissertation, Dept. of Meteorology, The Pennsylvania State University, 136 pp. [Available from http://etda.libraries.psu.edu/theses/approved/WorldWideIndex/ETD-4955/index.html.]

——, Y. Richardson, P. Markowski, J. Wurman, and D. Dowell, 2006: The maintenance of tornadoes observed with high-resolution mobile radars. Preprints, *23rd Conf. on Severe Local Storms*, St. Louis, MO, Amer. Meteor. Soc., 15.1.

——, Y. Richardson, J. Wurman, and P. M. Markowski, 2008: Single- and dual- Doppler analysis of a tornadic vortex and surrounding storm-scale flow in the Crowell, TX, supercell of 30 April 2000. *Mon. Wea. Rev*., **136**, 5017–5043.

——, Y. Richardson, P. Markowski, D. Dowell, and J. Wurman, 2011: The maintenance of tornadoes observed with high-resolution mobile Doppler radars. Accepted to *Mon. Wea. Rev.*

Marwitz, J. D., 1972: The structure and motion of severe hailstorms. Part I: Supercell storms. *J. Appl. Meteor*., **11**, 166–179.

——, and D. W. Burgess, 1994: The observed inflow structure of a thunderstorm with a mesocyclone. *Mon. Wea. Rev.*, **122**, 393–396.

Miller, L. J., J. D. Tuttle, and C. A. Knight, 1988: Airflow and hail growth in a severe northern high plains supercell. *J. Atmos. Sci.*, **45**, 736–762.

Okubo, K., 1970: Horizontal dispersion of floatable particles in the vicinity of velocity singularities such as convergences. *Deep-Sea Res*., **17**, 445–454.

Pauley, P. M., and X. Wu, 1990: The theoretical, discrete, and actual response of the Barnes objective analysis scheme for one- and two-dimensional fields. *Mon. Wea. Rev*., **118**, 1145–1163.

Rasmussen, E. N., and J. M. Straka, 2007: Evolution of low-level angular momentum in the 2 June 1995 Dimmitt, Texas, tornado cyclone. *J. Atmos. Sci.*, **64**, 1365–1378.

——, ——, R. P. Davies-Jones, C. A. Doswell, F. H. Carr, M. D. Eilts, and D. R. MacGorman, 1994: Verification of the Origins of Rotation in Tornadoes Experiment: VORTEX. *Bull. Amer. Meteor. Soc.*, **75**, 995–1006.

Ray, P. S., 1976: Vorticity and divergence fields within tornadic storms from dual-Doppler observations. *J. Appl. Meteor.*, **15**, 879–890.

——, R. J. Doviak, G. B. Walker, D. Sirmans, J. Carter, and B. Bumgarner, 1975: Dual-Doppler observation of a tornadic storm. *J. Appl. Meteor.*, **14**, 1521–1530.

——, B. C. Johnson, K. W. Johnson, J. S. Bradberry, J. J. Stephens, K. K. Wagner, R. B. Wilhelmson, and J. B. Klemp, 1981: The morphology of several tornadic storms on 20 May 1977. *J. Atmos. Sci.*, **38**, 1643–1663.

Richardson, Y., D. Dowell, and J. Wurman, 2001: High resolution dual-Doppler analyses of two thunderstorms during the pretornadogenesis and mature tornado stages. Preprints, *30th Int. Conf. on Radar Meteorology*, Munich, Germany, Amer. Meteor. Soc., 295–297.

Romine, G. S., D. W. Burgess, and R. B. Wilhelmson, 2008: A dual-polarization-radar-based assessment of the 8 May 2003 Oklahoma City area tornadic supercell. *Mon. Wea. Rev.*, **136**, 2849–2870.

Rotunno, R., and J. B. Klemp, 1985: On the rotation and propagation of simulated supercell thunderstorms. *J. Atmos. Sci.*, **42**, 271–292.

Shabbott, C. J., and P. M. Markowski, 2006: Surface in situ observations within the outflow of forward-flank downdrafts of supercell thunderstorms. *Mon. Wea. Rev.*, **134**, 1422–1441.

Shapiro, M. A., and D. Keyser, 1990: Fronts, jet streams and the tropopause. *Extratropical Cyclones: The Erik Palmén Memorial Volume*, C. W. Newton and E. O. Holopainen, Eds., Amer. Meteor. Soc., 167–191.

Shimizu, S., H. Uyeda, Q. Moteki, T. Maesaka, Y. Takaya, K. Akaeda, T. Kato, and M. Yoshizaki, 2008: Structure and formation mechanism on the 24 May 2000 supercell-like storm developing in a moist environment over the Kanto Plain, Japan. *Mon. Wea. Rev.*, **136**, 2389–2407.

Straka, J. M., E. N. Rasmussen, R. P. Davies-Jones, and P. M. Markowski, 2007: An observational and idealized numerical examination of low-level counter-rotating vortices in the rear flank of supercells. *Electronic J. Severe Storms Meteor.*, **2** (8), 1–22.

Trapp, R. J., 1999: Observations of non-tornadic low-level mesocyclones and attendant tornadogenesis failure during VORTEX. *Mon. Wea. Rev.*, **127**, 1693–1705.

——, and C. A. Doswell, III, 2000: Radar data objective analysis. *J. Atmos. Oceanic Technol.*, **17**, 105–120.

——, G. J. Stumpf, and K. L. Manross, 2005: A reassessment of the percentage of tornadic mesocyclones. *Wea. Forecasting*, **20**, 680–687.

Vasiloff, S. V., E. A. Brandes, R. P. Davies-Jones, and P. S. Ray, 1986: An investigation of the transition from multicell to supercell storms. *J. Clim. Appl. Meteor.*, **25**, 1022–1036.

Wakimoto, R. M., and N. T. Atkins, 1996: Observations on the origins of rotation: The Newcastle tornado during VORTEX 94. *Mon. Wea. Rev.*, **124**, 384–407.

——, and C. Liu, 1998: The Garden City, Kansas, storm during VORTEX 95. Part II: The wall cloud and tornado. *Mon. Wea. Rev.*, **126**, 393–408.

——, and H. Cai, 2000: Analysis of a nontornadic storm during VORTEX 95. *Mon. Wea. Rev.*, **128**, 565–592.

——, W.-C. Lee, H. B. Bluestein, C.-H. Liu, and P. H. Hildebrand, 1996: ELDORA observations during VORTEX 95. *Bull. Amer. Meteor.* Soc., **77**, 1465–1481.

——, C. Liu, and H. Cai, 1998: The Garden City, Kansas, storm during VORTEX 95. Part I: Overview of the storm life cycle and mesocyclogenesis. *Mon. Wea. Rev.*, **126**, 372–392.

——, H. Cai, and H. V. Murphey, 2004a: The Superior, Nebraska, supercell during BAMEX. *Bull. Amer. Meteor. Soc.*, **85**, 1095–1106.

——, H. V. Murphey, and H. Cai, 2004b: The San Angelo, Texas, supercell of 31 May 1995: Visual observations and tornadogenesis. *Mon. Wea. Rev.,* **132**, 1269–1293.

Ward, N. B., 1972: The exploration of certain features of tornado dynamics using a laboratory model. *J. Atmos. Sci.*, **29**, 1194–1204.

Weiss, J., 1991: The dynamics of enstrophy transfer in two-dimensional hydrodynamics. *Physica D*, **48**, 273–294.

Wicker, L. J., and R. B. Wilhelmson, 1995: Simulation and analysis of tornado development and decay within a three-dimensional supercell thunderstorm. *J. Atmos. Sci.*, **52**, 2675–2703.

Wurman, J., 2001: The DOW mobile multiple Doppler network. Preprints, *30th Int. Conf. on Radar Meteorology*, Munich, Germany, Amer. Meteor. Soc., 95–97.

——, J. Straka, E. Rasmussen, M. Randall, and A. Zahrai, 1997: Design and deployment of a portable, pencil-beam, pulsed, 3-cm Doppler radar. *J. Atmos. Oceanic Technol.*, **14**, 1502–1512.

——, Y. Richardson, C. Alexander, S. Weygandt, and P. F. Zhang, 2007a: Dual-Doppler and single-Doppler analysis of a tornadic storm undergoing mergers and repeated tornadogenesis. *Mon. Wea. Rev.*, **135**, 736–758.

——, Y. Richardson, C. Alexander, S. Weygandt, and P. F. Zhang, 2007b: Dual-Doppler analysis of winds and vorticity budget terms near a tornado. *Mon. Wea. Rev.*, **135**, 2392–2405.

——, K. Kosiba, P. Markowski, Y. Richardson, D. Dowell, and P. Robinson, 2011: Fine-scale single- and dual-Doppler analysis of tornado intensification, maintenance, and dissipation in the Orleans, Nebraska, supercell. *Mon. Wea. Rev.*, **139**, in press.

Xue, M., 2004: Tornadogenesis within a simulated supercell storm. Preprints, *22nd Conf. on Severe Local Storms*, Hyannis, MA, Amer. Meteor. Soc., 9.6.

Ziegler, C. L., E. N. Rasmussen, T. R. Shepherd, A. I. Watson, and J. M. Straka, 2001: The evolution of low-level rotation in the 29 May 1994 Newcastle–Graham, Texas, storm complex during VORTEX. *Mon. Wea. Rev.*, **129**, 1339–1368.

REVIEWER COMMENTS

[Authors' responses in *blue italics.*]

Overview of Major Changes

We thank all of the reviewers for their constructive comments. The reviewers have made an extraordinary effort to carefully review our paper, and we are grateful for their contributions.

The most significant criticisms were to better quantify uncertainty, present data over greater depths, and make more comparisons to tornadic cases, when possible. We have taken the criticisms to heart (the revised manuscript is substantially longer than the original, however). The revised manuscript goes to great lengths to quantify the uncertainty in all computations. Regarding the altitudes of the analyses presented, the revised manuscript now also better discusses the vertical variation of circulation characteristics, particularly in the presentation of azimuthal averages. With respect to comparisons to tornadic low-level mesocyclones, we have expanded the discussion of the tornadic versus nontornadic mesocyclone characteristics, although we feel as though a major longitudinal study awaits the completion of VORTEX2 case studies, given how limited the number of tornadic (and nontornadic) cases is at the time of this writing (especially before tornadogenesis in the case of the tornadic low-level mesocyclones).

REVIEWER A (David Dowell):

Initial Review:

Recommendation: Accept with minor revision.

Substantive Comments: The paper's important contribution is documenting nontornadic supercells, so that similarities and differences from tornadic supercells documented elsewhere can be identified. The figures are generally well designed. Section 3, consisting of a long list of observations with minimal synthesis, requires some endurance on the part of the reader. The paper lacks strong conclusions but attempts to raise good questions that eventually need good answers. The paper could be made stronger by organizing some of the discussion in sections 3 and 4 around the important questions that must be addressed in future studies.

1. Among the cases shown in Fig. 9, the most noticeable difference between nontornadic and tornadic cases appears to be in circulation for r <1 km. Therefore, consider emphasizing this point more in the abstract. At minimum, add a phrase such as "particularly for r <1 km" to lines 11-12 of the abstract.

Okay.

2. With scale analysis, it's easy to show that mesocyclone circulation >> tornado circulation for typical length and velocity scales associated with these phenomena. The suggestion in the abstract (lines 13-16) and in section 4 (paragraph 4) that mesocyclones (tornadic or nontornadic) have enough circulation to make a tornado is not a new result. Furthermore, the suggestion in the abstract that there was "probably" enough circulation seems unnecessarily uncertain. Recommended changes to the manuscript are (1) in section 4 paragraph 4, add a reference to previous work concerning mesocyclone and tornado scale analysis and implications, and (2) delete lines 13-16 ("although the nontornadic … large radius from the axis.") of the abstract.

With respect to (2), we've deleted the text in question. With respect to (1), after much deliberation, we feel that a comparison of tornado-scale circulation to mesocyclone-scale circulation gets away from our purpose (nor do we resolve tornado-scale motions, at least not in the dual-Doppler wind syntheses). Instead, we have added…clarifying text to the end of the paragraph in question in section 4.

[Text-body block from manuscript omitted…]

3. For this study, it is important to provide objective criteria for identifying tornadoes, so that it is clear how the distinction between nontornadic and tornadic supercells was made. It would be appropriate to provide this information early in section 1, perhaps paragraph 2 on p. 2. On p. 4, there is a suggestion

that the storms were considered nontornadic because the radial velocity differences across the mesocyclone at approximately 100 m AGL were <30 m s^{-1}, but it's unclear whether these criteria are the radar-based "tornado definition" used for this study. Also, for the criteria that were used, please verify that the tornadic storms (particularly the Argonia storm, which is likely to be the most marginal) indeed meet the criteria for being tornadic.

The paragraph in question has been rewritten/expanded.

4. The suggestion on p. 2 that only 20 or so dual-Doppler supercell cases exist seems way off. Aren't dual-Doppler supercell datasets, albeit at distant ranges and with coarse resolution, obtained numerous times every year by the WSR-88D network? And with richer instrument networks (e.g., central OK), aren't higher resolution dual-Doppler supercell datasets obtained multiple times per year? Furthermore, the suggestion that Table 1 contains the complete / nearly complete list of peer-reviewed supercell cases seems significantly off the mark. It's easy to find other examples in the peer-reviewed literature. Please reconsider the numbers provided in the manuscript and/or be more specific about how the short list of roughly 20 cases overall and 8 peer-reviewed cases was selected.

We've added a few cases to the list (we thank you for pointing out a few additional cases), and also been more clear in the text to acknowledge that it's practically inconceivable that we've identified them all.

5. On p. 3, right column, line 18, please mention how spatial resolution is defined.

The wording "spatial resolution" has been replaced with "data spacing."

6. Section 3 is quite long. Consider eliminating less important details, synthesizing results occasionally, and/or organizing the discussion around questions that could be (and must be) answered with better observations.

Thanks for the suggestion. We've improved the transitions between paragraphs and sections in places, which hopefully gives the reader some needed "breaks."

7. "Occluded" gust-front structures are mentioned several times in the paper: line 8 of the abstract, line 20 on p. 4, line 8 of section 3 on p. 8, and line 3 of the right column on p. 21. Furthermore, on p. 4 it is stated that "kinematically the wind field [redundant?] resembles the wind field of an extratropical cyclone." This reviewer is having difficulty seeing the resemblance. How do the single curved boundaries drawn on the figures relate to the cold front - warm front - occluded front structures in the typical model of an extratropical cyclone?

By "occluded" we mean that outflow has wrapped around the circulation center, cutting it off from the inflow sector at the surface, just as an occluded extratropical low is one that has been cutoff from the warm sector at the surface (the generic definition of "occlusion" is along the lines of "blockage" or "obstruction"). We have added a brief parenthetical remark to clarify our use of the term the first time it appears in the main body of the text. Regarding the use of the phrase "kinematically the wind field resembles…," we prefer to retain the wording lest a reader misunderstand us to be suggesting that the wind field resembles that of an extratropical cyclone in a kinematic and dynamical sense.

8. Excluding other cases for reasons that are "obvious" (next to last paragraph in section 1) seems nonscientific. How were cases really selected? Randomly? Based on strength of low-level rotation? Based on resemblance to tornadic supercell cases?

We chose to present only those cases for which strong near-surface rotation was observed, i.e., the cases that would likely present the greatest challenge to discriminate from tornadic storms. We did not present analyses of nontornadic supercells that had no low-level outflow (e.g., one case excluded was a dying LP storm); we believe such storms are nontornadic for the obvious reason that a downdraft is required in order for rotation to develop at the surface (in the absence of pre-existing rotation and on timescales too short for the Coriolis force to contribute significantly). We've reworded the paragraph in question to clarify our reasoning behind the case selection.

9. Do single-Doppler measurements confirm that low-level rotation had a maximum value at 0025 UTC in the Las Animas storm (cf. p. 6, right column, first paragraph)?

The first dual-Doppler volume was actually at 0024 UTC (not 0025 UTC as previously reported), and the maximum rotation was observed at 0025 UTC. There is no single Doppler evidence of stronger rotation at earlier times (the updraft and mesocyclone only developed during the 0005–0020 UTC period.

10. On p. 7, end of first paragraph, please be specific about how one can tell which data have been interpolated and which have been extrapolated.

Segments of material circuits that pass below the data horizon have been dashed in Fig. 8. In Fig. 7, the segments of the trajectories that pass below the data horizon are so short that they are not discernible in the figure (these trajectories have different origins than those in Fig. 8).

11. Other than w=0 at the ground (p. 7), were additional boundary conditions used to guarantee a unique solution from the upward-integration technique? It seems quite likely that some coplanar arcs within the region of dual-Doppler coverage do not terminate at the ground (i.e., the location where the w=0 boundary condition is specified) within the Cartesian domain.

No additional boundary conditions were used. We do not have any good strategies for how to specify w along the lateral sides of the domain. We verified the uniqueness of the solutions in the 12 June 2004 case by comparing them to retrievals derived from gridded radial velocity fields having no data boundaries along coplanar arcs that passed through the dual-Doppler region (these grids encompassed larger domains and were based on extrapolated data, where necessary, so that there would be no coplanar arcs terminating at data boundaries above the ground in the dual-Doppler region). The original retrievals were practically identical to the test retrievals. [Small differences (<15 cm/s in the retrieved u, v, and w wind components) are present, but these are unavoidable because the objectively analyzed reflectivity and radial velocity fields are themselves affected by the locations of data boundaries, i.e., changing the grid dimensions unavoidably affects the grid values (at least slightly), even for a relatively small Barnes smoothing parameter.] We did not repeat this experiment for the other cases, but have no reason to believe that there are pathological geometries or data holes in the other cases that have led to nonunique solutions.

12. On p. 7, right column, paragraph 2, please describe briefly the response function of the Leise filter.

Done.

13. Why was the Okubo-Weiss number (p. 8) chosen for identifying circulation centers rather than simply vorticity?

We've added a much better explanation for this approach in the revised paper.

14. Providing information on storm motion would be helpful in interpreting results for the three cases. Consider plotting the mean storm-motion vector on one or more figures.

We've included this in the revised text.

15. How relevant are the plots of circulation versus time in Fig. 8e? Is 1-4 minutes long enough to see important trends? Are the plots dominated by "signal" or "noise" (analysis errors)?

Error bars have been added to Fig. 8e. The error bars indicate one standard deviation of uncertainty. The uncertainty was estimated from 100 integrations of the trajectories comprising the material circuits, wherein the three-dimensional wind syntheses used to compute the trajectories were randomly perturbed in each realization, with the perturbations of the u, v, and w wind components having a Gaussian distribution, zero mean, and standard deviations of 1 m s^{-1}, 1 m s^{-1}, and 2(z/1000 m) m s^{-1}, respectively. The assumed u, v, and w uncertainties are comparable to the uncertainties obtained in the dual-Doppler experiments using synthetic radar data performed by Majcen et al. (2008; see their Table 2). Even a tripling of this uncertainty in u, v, and w would not obscure the trends shown in Fig. 8e. Circulation calculations along material circuits are surprisingly robust, despite the fact that errors in the computed circulation values result from errors in the position of the circuit and errors in the winds interpolated to the circuit (trajectory errors, as it turns out, are relatively small over short integration periods of just a few minutes, as long as trajectories do not pass very near to intense, translating vortices). The downside of using material circuits is that the circuits can take on very complex shapes, especially if the time-integrations are long.

16. In the final paragraph, please be more specific about why "thermodynamic and perhaps microphysics observations" are needed to improve our understanding of tornadic and nontornadic storms. What observations are needed, and how could they have helped in the current study?

We've tried our best to expand on the original remarks some more (although we're also wary of opening a new can of worms in the second-to-last sentence of the paper). Hopefully you'll view our modifications favorably.

[Minor comments omitted...]

Second review:

Recommendation: Accept.

General Comments: The authors have done an outstanding job responding to the reviews and getting the manuscript in good shape. I find the manuscript acceptable for publication in its current form. *[Minor comments omitted…]*

REVIEWER B (Erik N. Rasmussen):

Initial Review:

Reviewer recommendation: Revisions required.

This table summarizes my evaluation of this study. Specific comments follow the table.

Criterion	Satisfied	Deficient, but can be remedied	Deficient; cannot be remedied by modifying the paper	Deficient, *not known* if it can be remedied by modifying the paper
Does the paper fit within the stated scope of the journal?	✓			
Does the paper 1) identify a gap in scientific knowledge that requires further examination; 2) repeat another study to verify its findings; or 3) add new knowledge to the overall body of scientific understanding?	✓			
Is the paper free of errors in logic?		✓		
Do the conclusions follow from the evidence?		✓		
Are alternative explanations explored as appropriate?	✓			
Is uncertainty quantified?		✓		
Is methodology explained in sufficient detail so that the work could be reproduced by others?	✓			
Is previous work and current understanding represented correctly?		✓		
Is information conveyed clearly enough to be understood by the typical reader?	✓			

Substantive Comments:

Summary: This paper is very well written. It's always nice to be able to understand what is being conveyed without struggling through vague, imprecise, and ambiguous language. I hope the authors are able to pass along this trait to those under their tutelage!

You may have seen my little chart (above) before. It is my attempt to try to objectively apply the scientific method to the review process, and to maybe nudge the community just a bit away from the subjectivity and personality-based reviewing that I think has dominated for much too long. I think the EJSSM's Reviewer guidelines are a good step in the right direction as well. To my way of thinking, if the paper has adhered to the valid scientific methodology, and is comprehensible, it should be published. Although probably too simplistic, it seems to me that if an editor gets a chart back with marks all in the left-hand column, the paper is acceptable.

Issues/criticisms:

1. Las Animas storm discussion, p6. You cannot assert that this vortex was at its maximum strength if there is a gap in the temporal coverage, and then when scanning is resumed, the vortex is at its peak strength. I.e., you cannot refute the hypothesis that the max occurred while it was not being observed well. To remedy this, I would propose that you just acknowledge the possibility. As I think about this study, it was good methodology to try to find Trapp's "time of tornadogenesis failure", although even his definition/application is more a matter of convenience than physics, in my opinion. But I don't see how your conclusions could be affected in any important way by the uncertainty in the time of the max intensity for this vortex.

The first dual-Doppler volume was actually at 0024 UTC (not 0025 UTC as previously reported), and the maximum rotation was observed at 0025 UTC. There is no single Doppler evidence of stronger rotation at earlier times (the updraft and mesocyclone only developed during the 0005–0020 UTC period.

2. I like the detailed exposition of the wind analysis methodology. However, I am left a bit uncertain about the uncertainty. Please provide a citation for the method if you have one, where you first discuss the method, and make sure the cited literature adequately discusses uncertainty and pitfalls. This is marked in the first column on p. 7 in my marked-up version. I am in no way criticizing the overall approach and in fact I really appreciate the level of detail and the fact that that you are not making some of the mistakes that have occurred in the historical literature.

We have performed almost as many sensitivity tests as we can imagine (most resulted in less sensitivity than we might have guessed). We hope that the reviewer will be satisfied with the improved quantification of uncertainty.

3. I would like to see just a bit more rigor in the justification of neglecting fall speed. Especially, can an uncertainty bound be stated? And of course the big worry is that with the convolution of the hook echo and its large reflectivity gradients with the viewing angle, there is likely to be a spatial pattern to the errors in velocity. Is there any way to more formally demonstrate that you made the right choice here; i.e., that using a fall-speed correction even with poor reflectivity quantification is worse than assuming $w_t = 0$, or that your reasoning is correct that w_t is having a negligible effect on radial velocity?

Comparisons of wind syntheses in which fall speeds were parameterized in terms of the maximum reflectivity observed by the two radars at a grid point yielded only small differences [$O(10^{-2}$ m s^{-1}) RMSE for the wind components at 300 m AGL; $O(10^{-1}$ m s^{-1}) RMSE in a volume extending from 100 m AGL to 1500 m AGL]; thus, we can be confident that the neglect of fall speeds does not change any qualitative interpretation of the results.

4. The discussion concerning radial divergence is incorrect. Radial divergence is $(1/r)d/dr(rV_r)$. So divergence occurs where (rV_r) is increasing with radius, not simply where $V_r > 0$; i.e., it is the slope of the radial velocity profile, with some pretty substantial geometric amplification as a function of radius,

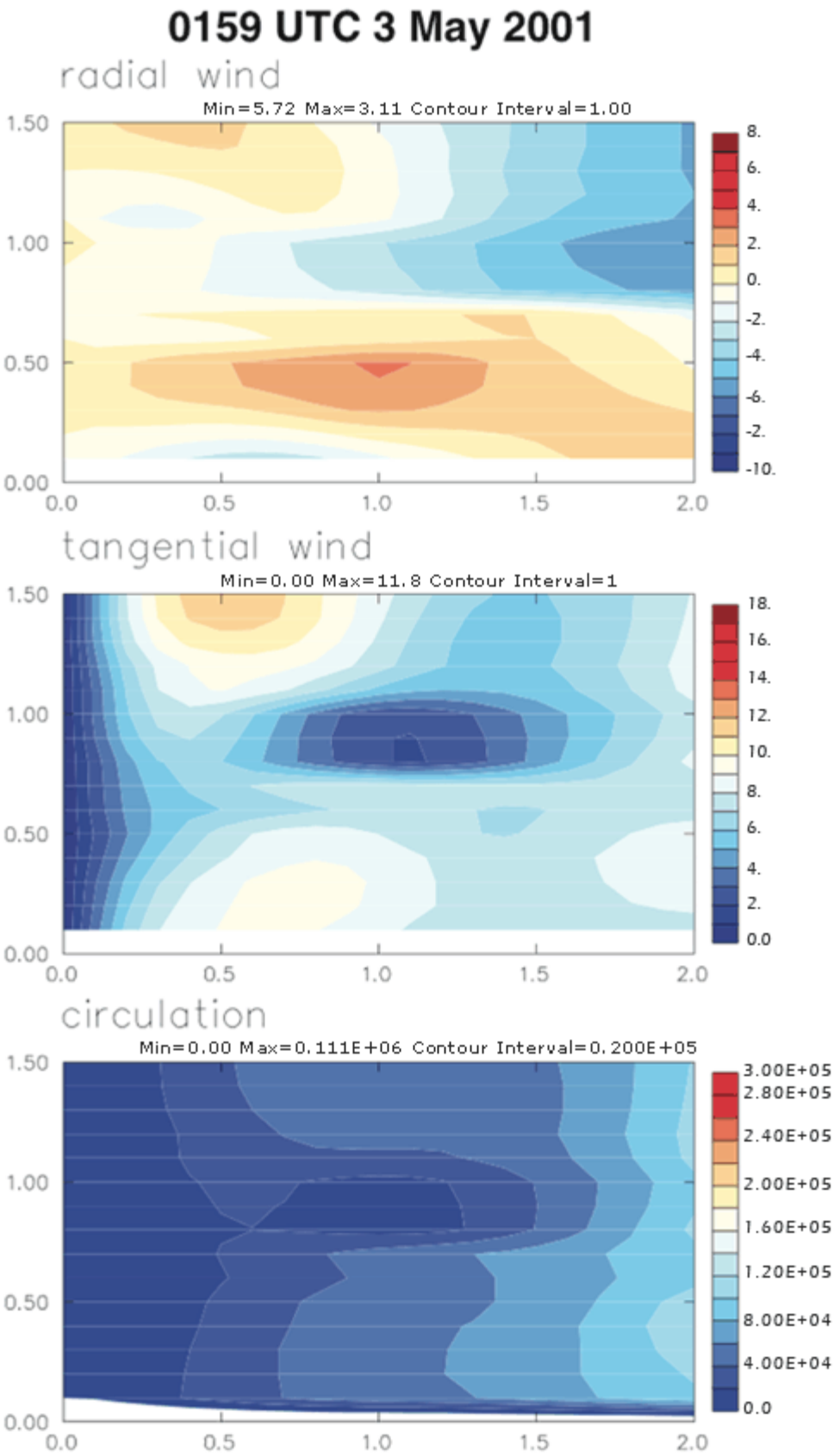
0159 UTC 3 May 2001
radial wind
Min=5.72 Max=3.11 Contour Interval=1.00
8.
6.
4.
2.
0.
-2.
-4.
-6.
-2.
-10.
tangential wind
Min=0.00 Max=11.8 Contour Interval=1
18.
16.
14.
12.
10.
8.
6.
4.
2.
0.0
circulation
Min=0.00 Max=0.111E+06 Contour Interval=0.200E+05
3.00E+05
2.80E+05
2.40E+05
2.00E+05
1.60E+05
1.20E+05
8.00E+04
4.00E+04
0.0
1.50
1.00
0.50
0.00
0.0
0.5
1.0
1.5
2.0

that determines divergence. It might be interesting to go ahead and plot divergence in a row of graphs, similar to the way that circulation has been plotted below tangential velocity. Fortunately, the essence of the conclusions of the paper is not affected by this small error. (Be sure to revisit the Conclusion regarding convergence to make sure it reflects the actual analysis; it probably does.)

Yes, the convergence at a point is given by the above expression. But the discussion in question is referring to fields in an area-averaged (azimuthal-averaged) sense. The area-averaged divergence within a ring of radius r *is proportional to the azimuthally averaged radial wind at r via Gauss' theorem.*

5. I am very concerned about the implications of the choice of 300 m AGL as descriptive of vortex dynamics in the azimuthal average discussion. If there is a frictional convergence near the ground, it is quite plausible that there is a compensating divergence just above the inflow layer, and this would quite possibly be near 300 m AGL. One possible remedy would be to examine multiple levels; perhaps a better approach would be to do a vertical average of u and v instead of a single-height analysis. A third alternative is to examine [r,z] profiles of these variables at the three times. Frankly, I don't think any eureka moments will ensue. But I do think that the single-height analysis at 300 m is potentially problematic enough to make it worth deleting unless the question can be resolved.

The revised manuscript presents vertical cross-sections of azimuthally averaged fields.

6. I hate to do this, because it might sound completely self-serving. But I think the Rasmussen and Straka (2007) JAS azimuthal average analysis is fairly pertinent. I am not sure why an analogous approach was not utilized (specifically, derivatives of the azimuthal average u, v components examined as a function of r, z, and t), because the data are certainly available in this study. The R/S analysis presented evidence that the temporal evolution of these fields was associated with vortex evolution, and vortex evolution is the topic of the current paper (so I am slightly puzzled why the R/S work was not cited or commented on). Of course, if the comments would have been highly critical, they are best left unsaid! Perhaps, for example, your data would reveal that these vortices were always dominated by a down/out average secondary circulation instead of the in/up associated with vortex intensification. Hence, I am suggesting that we could learn a little more from the present data set with that sort of analysis approach.

We have greatly expanded the presentation and discussion pertaining to the azimuthally averaged fields, and made comparisons to the Rasmussen and Straka (2007) study where appropriate. One major difference (challenge) for the nontornadic circulations—and we attempt to make this point in the revised manuscript as well—is that nontornadic circulations possess much less vertical continuity than an intense vertical vortex like a mature tornado. Defining the circulations centers is made difficult by large departures from axisymmetry, and this combined with significant horizontal shifts in the circulation centers with height can make vertical cross-sections of azimuthally averaged fields difficult to construct/interpret. At one stage of the revisions process, we attempted to construct vertical cross-sections by tracking the circulation center with height, even if it shifted horizontally by several km. We abandoned this approach because the cross-sections were practically uninterpretable (see below). Instead, we opted to keep the vertical axes upright, even if it meant that the axes only were centered in the near-surface rotation.

7. Conclusions, regarding trajectories: Do we have any historical evidence that low-level trajectories ever participate in mid-level mesocyclones, and if so, that this participation is associated with persistence in stretching? Your conclusion is not wrong, but perhaps it could use just a bit more qualification.

We've added more to this discussion. The short answer is yes, it seems that low-level trajectories in tornadic storms do reach high altitudes. This is based on trajectories in numerical simulations that produce intense surface vortices [e.g., Adlerman's Ph.D. thesis simulations of cyclic tornadogenesis, Xue (2004, SLS Conf. on Hyannis), Markowski et al. (2003, JAS), and Markowski et al. (2010, SLS Conf. in Denver)], as well as limited observations [e.g., the Argonia storm herein; the Friona storm in VORTEX1 exhibited a weak-echo hole from the lowest data levels all the way into the mid-upper troposphere—it's hard to envision how such a structure could result without low-level air reaching very high levels; moreover, on many occasions, light debris from tornadoes (e.g., canceled checks) is deposited far downstream].

Additional comments:

1. I sure got the sense in looking at your analyses that the typical fairly small domain of DOW dual-Doppler analysis is spatially and temporally insufficient for saying much about processes that depend on parcel history (e.g. circulation). It seems the circuits are out of the domain fairly quickly, which one would expect in the typically strong low-level supercell flow. Our VORTEX2 nesting concepts look pretty wise in retrospect, but one would still have to overcome the issues of radar horizon and the logistical issues of getting sufficient radars scanning at the same time. I don't know if you want to comment on this domain size issue or not; it's certainly not necessary.

Yes, there is a need for bigger dual-Doppler domains and longer time integrations. But the tradeoff with a larger dual-Doppler lobe is that there's not only less resolution, but the data horizon is higher. Backwards trajectories from a mesocyclone or tornado will quickly drop below the data horizon if the radar beams can't scan down to at least 100 m. With a 30-km baseline, roughly 50% of the dual-Doppler region has a data horizon [at or above] 400 m. That makes it almost impossible to do any backward trajectories without major extrapolation. We believe that the nested radar strategy proposed in VORTEX2 was exactly what was needed.

2. This is a well-written paper, and obviously a lot of hard work for a data set that did not yield any profound insights. Further, the authors are to be commended for not trying to generate profound conclusions when the atmosphere refused to provide them. Nice work.

Thanks for your thorough review.

[Minor comments omitted...]

Second review:

Recommendation: Accept, but give consideration to the following.

General Comments: This is a very good paper. I think in some ways it sets a standard for observational severe weather studies. In particular, the quantification of uncertainty was exactly what has been needed for the last several decades in this field. At last, we may be past the point of "trust me, I am an authority". I hope the authors found that the EJSSM approach is one that advances our science.

The analyses are well done and thorough, and the presentation graphics are concise.

The findings/conclusions follow well from the data, and the authors have exposed some very interesting avenues for future research that can take advantage of existing data sets.

I made a number of comments in the margins of the version I am returning. I encourage the authors to scan these, and see if any of them would lead to improvements or clarifications. The only change I would like to see before publication (although I don't insist on it; I am a lowly reviewer, after all) is that this item remaining from my previous review be addressed. It does not substantively change the conclusions…it is not an Achilles' Heel…but I think it is worth fixing given the otherwise great pains the authors took to quantify uncertainty! (Perhaps it is fixed, but I missed it on my first read, a second skim, and a search for the occurrence of "Animas" throughout the text.)

Las Animas storm discussion, p6. You cannot assert that this vortex was at its maximum strength if there is a gap in the temporal coverage, and then when scanning is resumed, the vortex is at its peak strength; i.e., you cannot refute the hypothesis that the max occurred while it was not being observed well. To remedy this, I would propose that you just acknowledge the possibility. As I think about this study, it was good methodology to try to find Trapp's "time of tornadogenesis failure", although even his definition/application is more a matter of convenience than physics, in my opinion. But I don't see how your conclusions could be affected in any important way by the uncertainty in the time of the max intensity for this vortex.

The Las Animas storm was not at its peak strength when scanning resumed. Scanning resumed before its peak strength was attained. The time given in the first version of the paper was incorrect and corrected in the second version. I believe you must have overlooked that.

We're grateful for all of the embedded comments in the electronic file. With respect to your objection about our description of the tornado cyclone being subjectively defined, Rasmussen and Straka (2007) write

"The tornado cyclone here is defined as a significantly axisymmetric flow larger than the visible tornado and characterized by increasing angular momentum with increasing radius."

That seems like an awfully subjective definition to us. Angular momentum increases with radius for all radii (this is a requirement of centrifugal stability), so that part of the definition does not help distinguish the tornado cyclone from the tornado or mesocyclone. That leaves "a significantly axisymmetric flow larger than the visible tornado"—it's not clear how one distinguishes this from the mesocyclone, if a distinction even exists.

With respect to the comment about closed streamlines enclosing regions of area-averaged w=0, the reviewer is correct. We did not mean for closed streamline being interpreted so literally, but the reviewer's interpretation is certainly reasonable. We've deleted the text in question.

REVIEWER C (Jana B. Houser):

Initial Review:

Reviewer recommendation: Accept with minor revisions.

Overview: In a field that generally focuses on the structure, environment, and evolution of tornadoes and their parent supercells, this paper provides valuable analyses of non-tornadic mesocyclones that resemble those of tornadic storms, with no obvious mode of tornadogenesis failure. The addition of such analyses to the current literature is welcome and greatly needed and extend the main conclusions of Vortex 1 (that on the storm-scale, tornadic storms cannot be discerned from nontornadic storms) to the sub-storm scale. The paper is well written and overall, my comments are rather minor.

Major Points: The only major concern I have with the content of the paper lies with the analysis of the third case storm (Las Animas). Dual-Doppler analyses are unavailable for ten minutes while the storm crosses the baseline between the DOWs. The paper made it seem like the authors defined the time of maximum mesocyclone strength immediately when analyses resume (i.e., as soon as the storm crosses back into the dual-Doppler lobe). They proceed to show that the mesocyclone rapidly weakened with time. My concern is that there is currently no evidence presented (or possibly available?) that would support the claim that the low-level mesocyclone was stronger at this time than during the time when the storm was crossing the baseline. If there are single-Doppler data available that can substantiate this claim (e.g. via radial velocity shear), please present this. Otherwise, this analysis may be misleading since it might not truly represent the mesocyclone at its peak intensity. Regardless, I feel it is necessary to draw the reader's attention to the fact that the results from this analysis should be viewed cautiously as the analysis may not truly represent the Las Animas storm at the strongest period of low-level rotation.

The description of the intercept of the Las Animas storm in section 2a has been rewritten (and lengthened) to include additional details of the deployment. The initial scanning target was a supercell to the west of the two radars. This storm displayed negligible low-level rotation and dissipated after entering the western dual-Doppler lobe formed by the north-south pair of radars. A new storm developed shortly after 0000 UTC right over the baseline and proceeded to move east into the eastern dual-Doppler lobe. The initial dual-Doppler synthesis of the low-level mesocyclone region is at 0024 UTC, not the 0025 UTC initially reported, and the vertical vorticity was a maximum at 0025 UTC.

[Minor comments omitted...]

Second Review:

Reviewer recommendation: Accept with minor revisions.

Overview: This revised manuscript is much more thorough and complete than the previous version. It is obvious that the authors put a considerable amount of time into the revisions and addressing the reviewers'

concerns. The addition of azimuthally averaged vertical cross sections and the comparisons between nontornadic and tornadic mesocyclones are a great asset to the revised manuscript and contribute to a much more complete story than previously. With that said, my comments are quite minor, and mostly semantic.

[Minor comments omitted...]

REVIEWER D (Jerry M. Straka):

Initial Review:

Reviewer recommendation: Accept with minor revisions.

This is a very interesting paper, which, though, probably serves modelers better by providing observations with which to compare with numerical simulation results, more than observationalists or modelers trying to understand details of tornadogenesis or the lack thereof with low-level mesocyclones.

After reading this paper I was left with the impression that tornadic low-level mesos and non-tornadic low-level mesos do not appear much different kinematically below 1000 m AGL, and particularly at 300 m AGL, using analyses from dual-Doppler data from the Doppler on Wheels systems. This implies very subtle difference between some low-level mesos that become tornadic and those that don't. Unfortunately, very little insight into why this might be is [provided]-only that VORTEX2 data may be more enlightening with regards to this issue, if I may paraphrase.

The biggest shortcoming of the paper, though, I believe, is suggesting to the reader such a conclusion such as the statement noted above about the how similar tornadic and non-tornadic low-level mesos might be, but only showing and writing about half of the story. I think the paper would have been much more convincing had at least two or three tornadic low-level mesos were shown doing the same analysis with the same observing systems. If the data are not available about tornadic low-level mesos or if they are available and have not been analyzed is this paper premature to present?

Limited comparisons of azimuthally averaged fields in tornadic and nontornadic low-level mesocyclones appear in section 3d (actually, you will probably be very pleased by the degree to which this section has been expanded, most notably, vertical cross-sections of azimuthally averaged fields are now presented). Unfortunately, there is just a dearth of pre-VORTEX2 dual-Doppler observations of tornadic low-level mesocyclones, especially prior to tornadogenesis (just as there is a dearth of dual-Doppler observations of strong nontornadic low-level mesocyclones, as implied by the fact that the present paper discussed three cases and not dozens of cases). We anticipate much better opportunities for comparisons (i.e., longitudinal studies) in the next 10-15 years as the VORTEX2 analyses roll off the presses.

In addition, the authors state a limitation of airborne data to be useful to only within 400 m AGL, yet they study only one level, which is 300 [m] AGL. As a result, the conclusions are left nearly completely out of context with regard to non-tornadic and tornadic low-level mesos. Admittedly, even without the analysis of three tornadic low-level mesos, some interesting conclusions can be and are drawn.

We chose to present fields at 300 m in order to maximize the data regions that could be shown (data generally exist down to 100 m in the vicinity of the circulation centers, but in the far reaches of the domain, the radar horizon is above 100 m—the entire analysis domain at 300 m is above the radar horizon). We note that the fields at 300 m are representative of those in the 0-1 km layer, i.e., there is little to be gained by presenting the same fields at additional levels. Trajectory and vortex line calculations, of course, extended all the way down to 100 m (or slightly below in some cases, as discussed in the text).

Some more major issues:

1. The discussion of mesocyclone detection problems with range is not required as this issue is and has been quite well known by researchers and forecasters alike for quite some time. On NOAA websites one can find the algorithm criteria for mesocyclone detection and possible tornado vortex signature (TVS) indication. The websites show that radial shear values for detection for both of these phenomena change with range.

We are unsure of the text in question, as we do not discuss mesocyclone detection problems as a function of range. The only sentence that mentions mesocyclone detection is in section 1, paragraph 1. Its purpose is to highlight the limitations of single-Doppler radar observations (which sets the stage for the presentation of the dual-Doppler observations presented herein) and to point out that there's more to tornadogenesis likelihood than simply mesocyclone strength (i.e., there may be discriminating traits of storms that are unobservable with single-Doppler data).

2. As noted above, the authors state a limitation of airborne data to only be useful within 400 m AGL (I think Roger Wakimoto has pushed it closer to the ground further than that, but how I don't know), yet the authors are content to show only one level, which is 300 m AGL. Claims of credible analyses at 100 m AGL only are discussed loosely and qualitatively. A difference of 100 m in height AGL (400 vs. 300 m AGL) is not all that significant. How close to the ground for non-tornadic and tornadic low-level mesos can really be studied with mobile system dual/multiple Doppler data collected from mobile systems. You write that it is 100 m AGL in this study. Some very useful contributions to modelers and observationalists alike could have been made had 100m AGL data been shown in this paper in addition to the 300 m data (we already have numerous 400 m figures in other papers to look at from other platforms.) I know 300 m probably was chosen as a compromise to showing data at 100 m and 1000 m. But still…

Regarding airborne datasets, the tilde that precedes "400 m" in the text is deliberate, i.e., we don't wish for readers to be too fixated on this precise elevation. The exact height depends, of course, on the altitude of the aircraft and on the vertical data spacing at the range of the storm. In severe storms projects like VORTEX1, the aircraft flies at ~300 m AGL and the vertical data spacing typically is 400-500 m at the range of the storm. Having unextrapolated data on a grid level 400 m above the ground is probably overly optimistic, actually. For example, Wakimoto et al. (1998), Wakimoto and Cai (2000), and Ziegler et al. (2002) didn't show horizontal cross sections below 600, 800, and 500 m, respectively. Regarding the issue of 300 vs. 400 m, we agree that this difference (and the differences between 300-400 m and 100, 600, and 800 m) is insignificant. For this reason, there's little to be gained from showing horizontal cross sections at these additional levels. What we see as the biggest drawback of having the lowest data level be in the 400-600 m range is the inability to compute trajectories—practically all trajectories that pass through the low-level mesocyclone would drop below the data horizon within seconds of backward integration. Some might also wonder about the importance of seeing close to the ground when it comes to vortex line calculations. E.g., a reviewer of the Markowski et al. (2008) paper (which was based on airborne Doppler radar observations) was skeptical that the vortex line "picture" wouldn't change if the data extended closer to the ground.

3. Could more about the circulations (using that word loosely) have been stated with use of single Doppler data much closer to the ground in conjunction with the dual-Doppler analyses, which maybe only are available within 100-300 m AGL.

The lowest data level of the single Doppler radar data is not much different than the lowest grid level with (unextrapolated) data at the range of the circulations (typically ~50-75 m vs. 100 m).

4. The discussion of tornadic and non-tornadic low-level mesos is an interesting topic alone in the context of the steadiness of overall storms. This issue is rarely discussed and is an interesting research topic, though perhaps this discussion need not be made without discussing low-level mesos containing tornadoes.

We refer to low-level mesocyclones as being tornadic or nontornadic whenever possible, as opposed to supercells being tornadic or nontornadic, precisely because of these labeling issues (e.g., a tornadic supercell is often nontornadic for much of, if not most of, its life).

5. The authors go to some length discussing the continuity of the data in space and time yet then retract and state that buoyancy retrievals were too "noisy" to be of any use, which would imply problems with local time derivatives and other derivative information as admitted by the authors. It is probably best to go with one story or another as the authors use much derivative information to identify circulation centers (deformation and vorticity) to computing low-level convergence and vorticity. Maybe more

explanation on this is required on this. I know a paper is referenced, and I am aware of the conclusions of Hane et al.

The differentiation involved in buoyancy retrievals is far more extensive than the differentiation required to obtain vertical velocity, deformation or vorticity. The latter involves taking single derivatives in space, whereas a buoyancy retrieval requires time derivatives and products of spatial derivatives [e.g., the vertical advection of vertical momentum is w(dw/dz), where w ultimately was derived by integrating the horizontal divergence] to evaluate the forces in the momentum equations, followed by another spatial differentiation to obtain the gradients of the sum of the forces, and then and additional vertical differentiation of the retrieved pressure perturbation.

6. In the conclusions (convergence section of the conclusions of the paper) why didn't you just do exactly what you wrote what you should have done and that is compare tornadic and non-tornadic low-level mesos.

The comparison of (area-averaged) convergence (proportional to azimuthally averaged radial velocity) in nontornadic and tornadic mesocyclones is presented in section 3d.

[Minor comments omitted...]

Second Review:

Reviewer recommendation: Accept.

I have reread the paper by Paul Markowski et al. and all the reviews of the paper and I am quite pleased at the revisions they made or the reasons they have given for not being compliant with requests (a detailed comparison of pre-tornadic and nontornadic low level mesos).

I suggest acceptance of the paper in the present form at this time…

[Minor comment omitted...]